Rheological Characterization of a Semi-solid Cream: Impact of Process Dynamics and Storage on Lamellar Gel Networks

Ruiqian Zhu

DIVISION OF FOOD AND PHARMA/CHEMICAL ENGINEERING | DEPARTMENT OF PROCESS AND LIFE SCIENCE ENGINEERING FACULTY OF ENGINEERING LTH | LUND UNIVERSITY
2026

Rheological Characterization of a Semi-solid Cream: Impact of Process Dynamics and Storage on Lamellar Gel Networks

Ruiqian Zhu

LUND
UNIVERSITY

Rheological Characterization of a Semi-solid Cream: Impact of Process Dynamics and Storage on Lamellar Gel Networks

Published by
Department of Process and Life Science Engineering
Faculty of Engineering LTH, Lund University
P.O. Box 118, SE-221 00 Lund, Sweden

Publicerad av
Institutionen för processteknik och tillämpad biovetenskap
Lunds Tekniska Högskola, Lunds universitet
Box 118, 221 00 Lund

Subject: KLGM06 Degree Project in Pharmaceutical Formulation

Division: Division of Food and Pharma/Chemical Engineerin
Supervisor: Marie Wahlgren
Co-supervisor: Cathrine Albèr
Examiner: Lars Nilsson

Ämne: KLGM06 Masterexamensarbete i läkemedelsformulering
Avdelning: Avdelningen för livsmedel och läkemedel/kemiteknik
Huvudhandledare: Marie Wahlgren
Examinator: Lars Nilsson

Rheological Characterization of a Semi-solid Cream: Impact of Process Dynamics and Storage on Lamellar Gel Networks

by

Ruiqian Zhu

Process and Life Science engineering

06 2026

Supervisor: Marie Wahlgren
Co-supervisor: Cathrine Albèr
Examiner: Lars Nilsson

A “Physical Examination” of the Microscopic World of Creams: How to Ensure a Perfect Tactile Sensation for Every Tube?

Why do some creams feel smooth and hydrating upon application, while others resemble stiff butter? The secret lies hidden within a microscopic “sandwich” structure invisible to the naked eye. We have identified a technology akin to “fingerprint recognition.” This technology can accurately diagnose whether a cream has been structurally compromised during industrial production. Consequently, it ensures that every tube delivered to patients is flawless.

Topical drug delivery is an extremely common treatment method in our daily lives. However, an excellent semi-solid cream is far from a simple mixture of water and oil. Its core consists of an extremely complex lamellar gel network. You can imagine this network as countless microscopic “sandwiches” formed by alternating layers of lipids and water. This three-dimensional sandwich framework traps a large amount of water and provides the cream with its solid form. Furthermore, it directly dictates whether the cream can melt instantly and spread smoothly upon contact with the skin. It also determines whether the active pharmaceutical ingredients can effectively penetrate the human skin barrier.

However, stably manufacturing these microscopic “sandwiches” in large-scale industrial facilities presents a massive challenge. The manufacturing process involves complex pipeline transportation, intense agitation, and rapid cooling. During these stages, a slight loss of temperature control or an excessively high pump speed can cause severe damage. These fragile microscopic frameworks can be torn, deformed, or grown into coarse agglomerates. Once the internal structure collapses, the cream exhibits severe macroscopic defects. It becomes extremely difficult to squeeze out and may undergo phase separation. This not only results a terrible user experience but also severely compromises the intended therapeutic efficacy.

To solve this industrial challenge, we successfully identified a method to conduct a “comprehensive physical examination” on these creams. By studying a commercial cream with a complex liquid crystalline structure (Zalve®), we established a set of “physical fingerprints” based on its perfectly healthy state. We intentionally manufactured defective creams in the laboratory by removing cooling equipment or omitting key components. During these tests, we discovered that this examination method could highly sensitively capture the pathological changes in their internal structures. This implies that pharmaceutical companies can simply perform basic physical tests during future continuous production. Just like taking an X-ray, they can instantly diagnose which specific step on the production line damaged the microscopic structure of the cream. They can precisely identify whether the cooling was too rapid or the mechanical squeezing was too intense. This capability will greatly assist factories in troubleshooting and reducing scrap rates.

During our research, we also discovered a fascinating detail. The cream is essentially alive! The internal structure of the cream is not permanently fixed immediately after filling on the production line. Over the following days, the product will slowly mature at room temperature. The microscopic crystals will spontaneously adjust their positions, becoming more densely packed and rigid. Just as wine requires time to settle, the cream typically undergoes physical aging to reach a more settled structural state.

To reach these conclusions, we primarily subjected the creams to precise “mechanical torture.” We did not utilize complex chemical reagents. Instead, we placed different batches of creams onto rheological instruments and applied precise compressive, tensile, and rotational shear forces. We observed their responses at the exact moment of initial flow and structural collapse. Furthermore, we combined these measurements with microscopes to capture vivid images of their internal crystals. Ultimately, these comprehensive data helped us decode the hidden relationship between the manufacturing process and the final microstructure.

Abstract

The macroscopic physical stability and clinical application performance of topical semi-solid formulations are highly dependent on the complex lamellar gel network (LGN) formed within their continuous phase. However, this microscopic three-dimensional scaffold exists in a thermodynamically metastable state and is extremely sensitive to kinetic parameters during the manufacturing process, such as thermal history and shear forces. This study aims to systematically evaluate the microstructural evolution and physical stability of a lipid-liquid crystalline system under various processing pathways, industrial scale-up stages, and long-term storage conditions, utilizing rheological characterization techniques combined with polarized light microscopy (PLM). This research compares steady-state industrial batches with laboratory and industrial samples exhibiting various process deviations. By conducting comprehensive rheological tests, including amplitude and frequency sweeps, yield stress determination, steady-state flow, and the three-interval thixotropy test (3ITT), and tracking the aging trajectory for several days, this study reveals the profound relationships between process, structure, and performance.

The results demonstrate that products reaching a thermodynamic steady state during continuous manufacturing exhibit a highly uniform birefringent microtexture, a moderate storage modulus (G'), and balanced thixotropic recovery. Early-stage process deviations and laboratory-scale extreme cases, such as missing key electrolytes or insufficient cooling and shear, produce coarse, anisotropic crystals or collapsed networks, which manifest rheologically as either elevated modulus or near-complete loss of solid-like behaviour. Rheological tracking during storage also revealed three distinct aging trajectories across the studied samples: the commercial Zalve® baseline showed an increase in storage modulus and a decrease in thixotropic recovery, qualitatively consistent with physical aging behaviour reported for related soft solid systems; whereas faulty production-line batches and freshly collected steady-state material followed different trajectories, with changes in yield stress and recovery rate that suggest structurally distinct relaxation pathways. The interpretation of these trajectories is tentative; absolute aging times differed between samples due to project-imposed timing constraints.

This study supports the use of multi-parameter rheology as a sensitive structural fingerprint for complex semi-solid formulations, with potential applications in Q3 structural equivalence assessment, process troubleshooting, and shelf-life evaluation of topical drug products.

Acknowledgement

Two years ago today, I wrote the acknowledgments for my bachelor's thesis in Nanjing. The summer there was so different from here. Even in early summer, the sun was already burning bright, and the heat was hard to bear. The humid air clung to my skin, and the cicadas sang endlessly through the day. Back then, I was fully prepared for my journey to Lund University. Like anyone else, I looked forward to the unknown, excited to cross thousands of kilometers to meet new people and experience new stories.

Two years in Lund have passed in the blink of an eye. I still remember the weather on the day I arrived. Sitting on the shuttle bus, I felt like this small town was a confusing maze. But now, I can take a leisurely walk through its streets without ever needing a map.

During the months of working on my degree project, I met many challenges, and there are so many people I want to thank. First, I want to express my deepest gratitude to my supervisor, Marie Wahlgren. Thank you for all your help, guidance, and encouragement, which brought me so much comfort during my anxious moments. You are so reliable and warm. Secondly, I want to thank my supervisor at Bioglan, Cathrine Albèr. Thank you for all your help and guidance. You are always so careful and patient, making me feel supported in an unfamiliar place. I am also truly grateful to Hanna Svensson at Bioglan. Without your preparation and help, it would have been very difficult to carry out many of my experiments. Thank you for being so kind and warm-hearted.

At the same time, I want to thank my supervisors and my examiner for their valuable advice and guidance. Thank you for helping me improve my thesis, making it my true masterpiece, and allowing me to learn so much from the process.

Life in Lund was a completely new beginning for me. Coming to a new country alone to start from scratch brought many hardships. I am deeply thankful to my classmates and the people who stayed by my side. Thank you for showing up and staying close, so I was never alone. You brought me a sense of home and warmth, helping me get through the freezing winter and giving me company on walks during beautiful spring days. Thank you for traveling with me to different cities in Europe, exploring new cultures and landscapes, and creating unique memories that belong only to us.

I also want to thank my parents from the bottom of my heart. Thank you for lifting me up so I could see a wider world, letting me experience the things I had only ever read about in books.

Finally, I want to thank myself. Thank you for becoming braver and stronger, and for opening your arms wider to embrace this world. I am grateful that everything I have been through has helped me grow.

Thank you to every spring day. It is so bright and dazzling, as if it can heal everything, making my eyes well up with tears.

Table Of Contents

1 Background 1
1.1 The challenge of semi-solid formulation 1
1.2 Guidelines 1
2 Aim of Thesis 3
3 Theoretical Background 4
3.1 Systematic Literature Review 4
3.2 Microstructure and Formation Mechanisms of Lamellar Gel Networks 5
3.3 Fundamentals of Rheological Characterization 6
3.4 Thermodynamics and Polymorphism of Lipid Crystallization 8
3.5 Maturation and Ageing of Gel Networks 9
4 Materials and Methods 11
4.1 Materials 11
4.2 Instrument and Equipment 11
4.3 Manufacturing Protocols 12
4.4 Analytical Characterization 13
4.5 Ageing and Storage Conditions 15
5 Results 16
5.1 Rheological Baseline: A Cross-Formulation Comparison 16
5.2 The Baseline: Micro- and Macro Properties of Commercial Zalve® 17
5.3 Microscopic and Rheological Behaviour of Two Laboratory-Scale Batches 20
5.4 Microstructural and Rheological Evolution during Industrial Scale-Up 22
5.5 Time Evolution Rheological Properties 25
6 Discussion 28
6.1 Defining Key Parameters at the Laboratory Scale: Formulation Integrity and Crystallization Thermodynamics 28
6.2 Industrial-Scale Production: Structural Evolution Along the Process Sequence 28
6.3 Evolution Under Storage Conditions: Three Distinct Aging Trajectories 29
7 Conclusion 31
8 Future Work 32
9 References 33
10 Appendix 35
10.1 Appendix A: Original results of polarized light microscopy 35
10.2 Appendix B: Full Rheology data 43

1 Background

1.1 The challenge of semi-solid formulation

Topical drug delivery serves as an essential clinical approach, playing a vital role in modern pharmaceutics. Compared to traditional oral administration, topical delivery exhibits distinct physiological advantages. These include enabling localized treatment to minimize systemic side effects and effectively avoiding first-pass metabolism, thereby improving drug bioavailability. However, the human stratum corneum acts as a highly dense natural barrier, hindering the penetration of drug molecules (Trommer, H, 2006). Therefore, designing formulation matrices capable of stably incorporating active ingredients and ensuring their effective release remains a core focus in the pharmaceutical industry (Ali, A, 2022).

Zalve® is a lipid-based carrier system built on mixtures of polar monoglycerides, primarily glycerol monolaurate and glycerol monomyristate, dispersed in excess water. Monoglycerides can self-assemble into ordered structures in aqueous environment, including crystalline, gel and liquid-crystalline phases depending on composition and temperature. It features a lamellar phase structure at the microscopic level, formed by alternating lipid bilayers. This lamellar gel network not only provides the product with excellent physical stability and viscoelasticity, but also directly influences its sensory properties upon application and drug release kinetics. However, this microstructure is sensitive and dynamic, and its formation is highly dependent on the kinetic conditions during the manufacturing process (Fukushima, S.,1997).

This project is the result of a close collaboration between Lund University and Bioglan AB. As a leading company focused on topical pharmaceuticals, Bioglan AB aims to optimize its production processes. Variations in manufacturing process parameters throughout the product lifecycle, ranging from laboratory and pilot-scale formulation development to continuous industrial production, can result in deviations in a product's microstructural integrity. Consequently, there is practical value in utilizing advanced rheological characterization to systematically evaluate these "process-structure" deviations. Furthermore, this approach will provide Bioglan AB with critical scientific insights for continuous process optimization, ultimately ensuring the consistency of the final steady-state product.

1.2 Guidelines

In 2018, the EMA published the Guideline on quality and equivalence of locally applied, locally acting cutaneous products. In Section 4.2.5, the EMA explicitly states that to establish extended pharmaceutical equivalence between a test product and a reference medicine, a detailed comparison of physical properties is required. The guideline mandates that this product characterization should include rheological characterization (EMA, 2018). This regulatory requirement highlights the essential role of rheology within the European framework, signifying that for complex semi-solid formulations, rheological data is recommended to be utilized to verify the consistency of their internal microstructures.

Beyond the European regulatory framework, the US Food and Drug Administration (FDA) demonstrated a highly consistent regulatory direction in its 2022 draft guidance, Physicochemical and Structural (Q3) Characterization of Topical Drug Products Submitted in ANDAs. Section 5 of this guidance focuses on defining the criteria for "Q3 characterization," clearly stating

that precise testing is necessary to demonstrate “structural sameness” regarding the arrangement and state of matter (FDA, 2022).

In summary, both the EMA’s direct requirement for rheological characterization and the FDA’s emphasis on Q3 structural sameness highlight that advanced rheological testing is a valuable tool for evaluating the microstructure of complex semi-solid formulations. Therefore, utilizing comprehensive rheological profiling is not only a scientific necessity for investigating physical properties, but also a crucial prerequisite for ensuring process consistency and regulatory compliance during industrial scale-up.

2 Aim of Thesis

The primary aim of this research is to systematically evaluate the microstructural stability of the complex lipid liquid crystalline system (Zalve®), across dimensions of process parameters, thermal history and storage time, utilizing advanced rheological characterization techniques.

To accomplish this goal, the thesis establishes the following four specific scientific and technical objectives:

1. Establishment of industrial steady-state characteristics: To define the rheological fingerprint of the lamellar network at a thermodynamic steady state during continuous industrial production. This baseline will serve as the gold standard for evaluating microstructural equivalence and process deviations.

2. Evaluation of deviations in manufacturing process parameters: To investigate how variations in processing conditions, including shortened residence times during transient start-up phases or deviations in cooling control, impact the self-assembly properties of the lamellar gel network at a microscopic level. This objective aims to reveal the structural sensitivity of the network to variations in shear and thermal history.

3. Assessment of inter-batch reproducibility for Q3 equivalence: To evaluate the reproducibility of the rheological fingerprint across independent industrial batches at multiple process states, thereby verifying the suitability of this multi-parameter protocol for Q3 structural equivalence assessment.

4. Analysis of network structure evolution and storage stability: To characterize the temporal evolution of the lipid liquid-crystalline network during long-term storage. By comparing the rheological responses at various time points, this objective seeks to identify potential structural maturation or polymorphic transitions occurring within the system post-production.

3 Theoretical Background

Zalve® is built on monoglycerides as the amphiphilic structurant, in combination with PEG-100 stearate as a non-ionic co-surfactant. The majority of the academic literature on lamellar gel networks in pharmaceutical and cosmetic creams, however, has been developed on fatty-alcohol systems, which share the same underlying colloidal architecture, alternating amphiphile bilayers separated by osmotically swollen water layers, but differ in the chemistry of the structurant and in the specific polymorphic terminology. The following sections therefore draw on both bodies of literature: the fatty-alcohol literature for the general LGN architecture and the well-characterised effects of cooling and shear, and the monoglyceride literature for the structurally analogous α-gel/coagel framework that applies directly to Zalve®. These references are used as conceptual frameworks for interpreting the rheological behaviour observed in this study, not as quantitative predictors of specific transition temperatures or d-spacings, which depend on the particular amphiphile chemistry.

3.1 Systematic Literature Review

To establish a robust theoretical framework for thoroughly understanding the process-structure-performance relationship of the Zalve® formulation, this study conducted a structured literature review. This approach ensures that the subsequent theoretical discussions regarding rheological principles, lipid crystallization dynamics, and the impact of manufacturing processes are all founded on high-quality, peer-reviewed scientific evidence.

3.1.1 Search Strategy and Database Selection

The Web of Science Core Collection was selected as the primary database for this research to guarantee the academic rigor of the literature sources. To comprehensively capture literature at the intersection of pharmaceutical engineering, colloid science, and thermodynamics, an advanced search strategy utilizing Boolean logic operators and wildcards (*) was employed. Specifically, the following two core search strings were constructed:

- Basic structural rheology search: (“lamellar gel network” OR “cetostearyl alcohol”) AND (“rheology” OR “viscoelasticity” OR “yield stress”)

  This search aims to collect classical theories explaining the formation mechanisms of lamellar gel networks and their fundamental rheological characteristics. Although the target formulation (Zalve®) is primarily based on monoglycerides rather than fatty alcohols, cetostearyl alcohol remains the most extensively documented and classically studied model component in LGN literature. Therefore, this term was intentionally included to capture the foundational physical theories, such as bilayer assembly and swelling mechanisms, which serve as essential conceptual analogues for understanding the target system.

- Thermodynamics and process dynamics search: (“lamellar gel network” OR “lipid crystallization” OR “fatty alcohol”) AND (“cooling” OR “thermal history”) AND (“rheology” OR “yield stress”) NOT (“alloy*” OR “titanium” OR “metal*” OR “steel”)

  In this search string, the NOT operator was intentionally introduced to exclude studies from the field of metallurgy. Similarly, "fatty alcohol" was included as a primary search keyword because the specific polymorphic transitions and crystallization dynamics driven by thermal history have been most rigorously characterized in fatty-alcohol-based LGNs.

Reviewing these classical models provides the necessary theoretical scaffolding to interpret the structural sensitivity of the monoglyceride-based network investigated in this study.

3.1.2 Inclusion and Exclusion Criteria and Results

The systematic search yielded highly targeted results. The first search generated 52 publications, which established the foundational theory of lamellar networks. The second search, focusing on cooling dynamics, retrieved 27 precise results.

Subsequently, a strict "funnel-like" screening procedure was implemented. All patent documents and studies originating from the food science sector, such as those regarding margarine or chocolate crystallization, were excluded to maintain an academic focus strictly on pharmaceutical and cosmetic topical formulations. Ultimately, a core set of academic papers was identified. These selected publications constitute the theoretical backbone for the subsequent subsections, specifically serving to explain how process dynamics dictate the microscopic assembly process and the macroscopic physical stability of semi-solid formulation networks.

3.2 Microstructure and Formation Mechanisms of Lamellar Gel Networks

In complex topical semi-solid formulations, macroscopic high viscosity, solid-like characteristics, and yield behaviour do not solely originate from the mechanical packing of dispersed droplets. Instead, they are dictated by a complex three-dimensional microstructure formed within the continuous phase: the lamellar gel network (LGN).

3.2.1 Definition and Self-bodying Action

According to Ribeiro et al. (2004), the semi-solid properties of many oil-in-water (O/W) creams are conferred by a highly swollen lamellar gel network in the continuous phase. This network is typically formed through the interaction of aliphatic amphiphiles, like cetyl or cetostearyl alcohol, and ionic or non-ionic surfactants in water.

Barry and Saunders (1970) showed that mixed emulsifiers such as cetrimonium bromide and cetostearyl alcohol exhibit a "self-bodying" action in the aqueous phase, forming a viscoelastic three-dimensional scaffold that traps water in the continuous phase and converts a low-viscosity liquid mixture into a stable semi-solid matrix (Barry & Saunders, 1970; Ribeiro et al., 2004).

3.2.2 Swollen Lamellar Phase and Water Interlayers

The microscopic essence of an LGN is an alternating "sandwich" structure. When surfactants insert into the fatty alcohol bilayers, their hydrophilic head groups form a charged layer on the bilayer surface. Due to electrostatic repulsion between like charges and the osmotic pressure of the hydrophilic groups, a substantial amount of water is strongly drawn between the bilayers, forming highly swollen "water interlayers." Using small-angle X-ray scattering (SAXS), Awad et al. (2011) determined that the repeating spacing (d) in such typical ternary systems often reaches approximately 30 nm. Although non-ionic systems tend to show somewhat smaller spacings due to weaker electrostatic repulsion, this order of magnitude illustrates how a significant fraction of the water is osmotically and electrostatically trapped between the bilayers, while additional bulk water occupies the gaps between LGN domains. The combined effect of this interlamellar confinement and inter-domain water entrapment is the physical root of the high elastic modulus (G') exhibited by semi-solid formulations (Ribeiro et al., 2004; Awad et al., 2011).

3.2.3 Intermolecular Interactions and Chain Length Matching

The stability of this structure relies heavily on the molecular ratio and geometric compatibility between the surfactant and the fatty alcohol. Research by Barry and Saunders (1970) demonstrated that the strongest gelation effect is induced only when the surfactant and fatty alcohol reach a specific molar ratio.

Awad et al. (2011) further revealed the importance of chain length matching. When the carbon chain length of the surfactant matches that of the fatty alcohol, the van der Waals forces within the bilayer are maximised, resulting in the tightest packing. If the component ratio deviates from the optimum, the packing becomes less ordered, the bilayers are less able to swell and retain water, and the mechanical properties of the network deteriorate accordingly.

3.2.4 Thermodynamic Pathways: Phase Transition Dynamics

The formation of a lamellar gel network is a process highly dependent on thermodynamic pathways. As described by Fukushima et al. (1977) and Awad et al. (2011), this process involves a transition from a liquid-crystalline phase (Lα) to a gel phase (Lβ):

- Lα phase: The alkyl chains of the fatty alcohols are in a disordered, highly fluid state.
- Lβ phase: When the temperature drops below the melting temperature (Tm) of the fatty alcohol chains, the alkyl chains undergo chain freezing, transforming into a highly ordered, crystal-like state.

  If the cooling rate is too rapid or the cooling process is interrupted, the fatty alcohol molecules may not align in time, leaving a discontinuous network or many unstable micronuclei. This gives a product with poor macroscopic rheological performance (Fukushima et al., 1977; Awad et al., 2011)

3.2.5 Structural Maturation and Aging

Because the LGN is a thermodynamically metastable system, its structure continues to evolve over time after production. Barry (1972) noted that the mechanical strength of the gel network often exhibits a continuous upward trend for hours or even days following its formation.

This maturation phenomenon is attributed to two factors: first, the fine-tuning and rearrangement of fatty alcohol molecules within the bilayer to reach a minimum energy state; second, the gradual equilibration of the water interlayer thickness driven by osmotic pressure. Furthermore, Fukushima et al. (1977) showed that polymorphic transitions of the fatty alcohol may also occur during storage, driving the structure from a less stable form to a more stable one. Therefore, evaluating the rheological response of the product at different time points is crucial for understanding its long-term physical stability and predicting its shelf life (Barry & Saunders, 1972; Fukushima et al., 1977).

3.3 Fundamentals of Rheological Characterization

The macroscopic mechanical behaviour of semi-solid formulations reflects their microstructural state. Rheology therefore serves both as an endpoint quality metric and as a sensitive probe for detecting network integrity and process deviations such as slow cooling or excessive shearing. This study uses both oscillatory rheology and steady-state rotational rheology (viscometry) to characterize the physical properties of Zalve®.

3.3.1 Linear Viscoelasticity and Dynamic Moduli

As discussed by Goggin et al. (1999), when a ternary gel system is subjected to small amplitude oscillatory shear, its response adheres to the theory of linear viscoelasticity. In this mode, the geometry does not rotate continuously; rather, it oscillates reciprocally in a sinusoidal wave pattern within an extremely small angle. When a sinusoidal strain $\gamma(t) = \gamma_0 \sin(\omega t)$is applied to the sample, the resulting shear stress $\tau(t) = \tau_0 \sin(\omega t + \delta_0)$ exhibits a certain phase lag (δ):

$$\tau(t) = \gamma_0[G'(\omega) \sin \omega t + G''(\omega) \cos(\omega t)]$$

By resolving this equation, the core moduli that describe the elastic and viscous characteristics of the network can be defined:

- Storage Modulus (G'): Represents the elastic energy stored and completely recovered by the material during deformation. Within a lamellar gel network, G' directly reflects the strength of the amphiphile bilayer scaffold. Ribeiro et al. (2004) noted that for a stable semi-solid cream, G' is typically approximately one order of magnitude higher than the loss modulus G", exhibiting significant solid-like characteristics.

- Loss Modulus (G"): Represents the energy dissipated as heat by the material during deformation.

The physical nature of the material can be intuitively determined through the loss tangent, $\tan \delta = G''/G'$. When $\tan \delta < 1$, the system behaves as an elasticity-dominated gel state.

3.3.2 Amplitude Sweeps and LVR

To ensure that the microstructure is probed without causing damage, the linear viscoelastic region (LVR) must first be identified. Within the LVR, the dynamic moduli G' and G" remain independent of the applied strain. Goggin et al. (1999) reported the critical strain values for cetostearyl alcohol ternary gels and showed that once the strain exceeds this limit, the non-covalent interactions between the bilayers begin to break down. For Zalve®, the width of the LVR can therefore indicate the structural integrity of the network formed under different process conditions.

3.3.3 Frequency Sweep and Structural Stability

A frequency sweep conducted within the LVR probes the time-dependent behaviour of the network. A well-developed lamellar gel network behaves as a true gel: G' forms a flat plateau across the tested frequency range and remains well above G", indicating that the three-dimensional scaffold is stable on multiple time scales. If G' decreases noticeably at low frequencies, the network may not be fully cross-linked or may contain structural inhomogeneities from incomplete crystallization.

3.3.4 Yield Stress Test

The yield stress is the minimum shear stress needed for the material to start flowing. It determines whether Zalve® holds its shape in the tube under gravity and resists phase separation during storage. Process deviations such as uncontrolled cooling rates can lead to a disordered bilayer arrangement, which is often reflected in a lower yield stress value.

3.3.5 Flow Curve and Shear Thinning

Once the applied stress exceeds the yield point, the flow behaviour is captured in a flow curve, which records viscosity as a function of shear rate. Lamellar-structured semi-solid creams are

typically pseudoplastic (shear-thinning) fluids, as the shear rate increases, the lipid bilayers align along the flow direction and slip past one another, causing viscosity to fall (Ribeiro et al., 2004).

3.3.6 Rotational Thixotropy and 3ITT

Lamellar gel networks exhibit time-dependent behavior. To simulate the destructive impact of high shear forces during actual production, such as pumping and filling, and the subsequent structural recovery, this study employs a Three Interval Thixotropy Test (3ITT) in continuous rotational mode (R-R-R mode). This test records the evolution of viscosity through step changes in the shear rate:

- First interval (low shear): Determines the initial resting viscosity of the sample.
- Second interval (high shear): Simulates smearing, where the viscosity drops sharply due to network breakdown.
- Third interval (recovery period): Records the kinetics of viscosity recovery over time.

The recovery ratio (η_3/η_1) quantifies how completely the network rebuilds after high-shear breakdown. A low recovery ratio indicates irreversible structural damage, while a high ratio suggests that the non-covalent bonds between bilayers can reform quickly. This metric is particularly sensitive to processing history because networks formed under suboptimal cooling or shear conditions tend to be more fragile and recover less completely.

3.4 Thermodynamics and Polymorphism of Lipid Crystallization

In Zalve®, the macroscopic properties of the lamellar gel network depend heavily on the crystallisation state of the lipid molecules, which is governed jointly by thermodynamics and kinetics.

3.4.1 Polymorphism

Lipid-based LGNs are thermodynamically metastable, and the crystalline state of the amphiphile bilayers continues to evolve after the network is formed. The classical framework, developed in fatty-alcohol systems by Fukushima et al. (1977), describes the α-form as the metastable, hydrated crystalline state present immediately after cooling, which transforms over time into denser β- (or γ-) forms with reduced capacity to retain interlamellar water.

An analogous framework exists in monoglyceride-based systems and is directly relevant to Zalve®. On cooling below the Krafft temperature, monoglycerides in excess water form a hexagonally chain-packed lamellar bilayer phase, referred to as the α-gel, which is metastable and progressively transforms during storage into the denser coagel phase, where the bilayers pack as β-crystals and a fraction of the interlamellar water is released (Heertje et al., 2005). The kinetics of this transition depend on cooling rate, applied shear, and the type and concentration of co-surfactants (Wang & Marangoni, 2015). In this thesis, the fatty-alcohol polymorphism literature is therefore used as a conceptual framework, while the monoglyceride α-gel / coagel literature provides the closest chemically appropriate references for Zalve®. Specific transition temperatures, d-spacings, and chain-length-matching parameters from either body of literature are not used as quantitative predictors.

3.4.2 Cooling Rate and Phase Transition

Crystallization kinetics are primarily governed by the cooling rate. Awad et al. (2011) indicated that when cooling from a temperature above the melting point, the system undergoes a transition from a liquid-crystalline phase to a gel phase.

- Controlled slow cooling: Molecules have sufficient time to overcome the energy barrier and develop a tightly packed crystalline bilayer structure. This continuous process builds a high-modulus lamellar scaffold.

- Rapid or uncontrolled cooling: The system becomes kinetically trapped in a less-ordered, metastable crystalline state. Alternatively, the rapid generation of crystallization nuclei leads to extremely small and discontinuous crystals.

3.4.3 Shear Induced Crystallization

Using Rheo-SANS on cetostearyl alcohol / cationic surfactant systems, Fameau et al. (2024) showed that the cooling rate and the applied shear during cooling jointly control the lateral packing of the bilayers and the formation of multilamellar vesicles. Moderate shearing helps break down excessively large crystal agglomerates and promotes a more uniform lamellar network. However, if the shear is poorly coordinated with the crystallization temperature, it may permanently disrupt the forming bilayer planes.

3.5 Maturation and Ageing of Gel Networks

After shearing and active cooling end, the LGN does not immediately reach its final state. The network is thermodynamically metastable and continues to evolve during post-production storage, which is a process commonly called gel maturation or ageing.

3.5.1 Structural Rearrangement and Thermodynamic Equilibrium

Network ageing post-production is primarily governed by relaxation dynamics at the molecular level. As shown by Fukushima et al. (1977), fatty alcohol molecules frozen in a higher-energy state during processing, such as the α-form generated by rapid cooling, will spontaneously transition into lower-energy, stable crystal forms during storage. Concurrently, molecules within the bilayer structure undergo subtle spatial rearrangements to optimize van der Waals forces and hydrogen bonding interactions. In the continuous phase, the osmotic pressure of water molecules and the electrostatic repulsion between the polar head groups of the surfactants also require time to reach a final dynamic equilibrium.

3.5.2 Time-dependent Rheological Behavior

The maturation process at the microscopic level directly maps onto the time-dependent macroscopic rheological characteristics. Barry and Saunders (1972) explicitly stated in their study of mixed fatty alcohol emulsifier systems that the consistency and mechanical moduli of the gel network exhibit a non-linear growth trend for hours or even weeks after formation. In oscillatory rheology tests, this ageing phenomenon typically manifests as a significant increase in the storage modulus and yield stress over time.

3.5.3 Amplification of Processing Defects

Ageing can also expose and amplify early processing defects. If the initial crystalline network is poorly developed, it will not form a continuous scaffold during storage. Instead, the structural defects may drive irreversible polymorphic transitions toward the denser coagel phase, which packs too tightly to retain interlamellar water and can lead to macroscopic phase separation or

syneresis. Measuring rheological parameters at different time points is therefore necessary to assess the processing quality of Zalve® and predict its shelf life.

4 Materials and Methods

4.1 Materials

This study focuses on the characterization and evaluation of the Zalve® topical semi-solid formulation. The samples investigated in these experiments are divided into two main systems:

- Industrial Scale Batches: This category includes three batches provided directly from the active industrial production line at Bioglan AB. These samples are utilized to evaluate how process drifts, pipeline retention, and filling-induced shear forces within a real manufacturing environment impact the microstructural characteristics of the final product.

  Sample C: the standard reference for the study. This sample was taken about 20 minutes into steady-state production at normal pump speed. It is a qualified bulk product that meets release standards but has not gone through the final tube filling step.

  Sample A: taken after the second cooling step at 33.6 °C, before the system had completed the full cooling profile. At this temperature, the lipid network is still partly in a liquid-crystalline state. The sample was collected during the first 30 kg of discharge, so the pump speed was higher than nominal and residual water from the previous cleaning cycle may have entered the mixture. Macroscopically, Sample A has a hardness similar to stiff butter.

  Sample B: taken after the final cooling step at 26.5 °C, during the initial discharge of the production run. Like Sample A, it was collected within the first 30 kg of material, so the pump speed was higher than during steady-state operation. Sample A, B, and C therefore represent three distinct process states (incomplete cooling, complete cooling but transient discharge, and steady state), not a sequential time series along the production line.

  To specifically evaluate the impact of extrusion shear during clinical application, a portion of Sample C was manually filled into standard Zalve® tubes (referred to as “Sample C in tube”) and allowed to rest prior to subsequent rheological testing.

- Laboratory Scale Batches: To more precisely isolate and investigate the impact of specific cooling pathways on the development of the gel network, two control batches were prepared in a laboratory setting:

  Batch 1: Zalve formulation composed of monoglycerides in excess water, propylene glycol, PEG-100 stearate and buffer agents. This batch utilized an external circulating water bath to achieve forced rapid cooling. But the ingredients are incomplete, which means the formulation is simplified.

  Batch 2: Same composition as Zalve. Manufactured with slow cooling.

4.2 Instrument and Equipment

The core equipment utilized in this study for formulation synthesis, rheological characterization, and microscopic evaluation is detailed below:

- Reactor for Batch 1: This batch utilized an IKA jacketed laboratory glass reactor system (IKA LR-2.ST system, IKA-Werke, Germany). This system is equipped with an IKA

EUROSTAR overhead stirrer. Furthermore, it is connected to an independent external heating and cooling circulator. This specific configuration enables precise and rapid heat exchange.

- Reactor for Batch 2: In contrast, this batch employed an IKA LR 1000 control integrated laboratory reactor system (IKA-Werke, Germany). This unit utilizes an integrated metal heating block at the base for temperature regulation. No external forced cooling jacket was applied, hence relying entirely on passive heat dissipation to achieve a slow cooling profile.

- Rotational Rheometer: A Kinexus series rotational rheometer (Malvern Instruments, UK) was employed for mechanical testing. It is equipped with a high-precision, integrated lower-plate temperature control system.

- Optical Microscopy Imaging System: An Olympus transmission optical microscope was utilized. It is specifically equipped with detachable cross-polarizing filter attachments. These specialized components include a polarizer positioned above the light source and an analyzer inserted above the objective lens.

4.3 Manufacturing Protocols

4.3.1 Labrotory Scale Batches

To investigate the impact of varying thermal histories on the final product, two distinctly different cooling and crystallization protocols were designed. These protocols were based specifically on the hardware characteristics of the two laboratory setups:

- Batch 1(800g scale): First, purified water was added to a jacketed IKA LR-2.ST reactor and heating was initiated. Subsequently, the aqueous phase excipients were added. Once the mixture temperature rose above approximately 60 °C, the solid oil phase lipid components and the remaining excipients were introduced directly into the reactor. The system was further heated to 70 °C - 75 °C to ensure the complete melting of all lipid components within the vessel. A mild vacuum environment of approximately 700 mBar was applied. Before crystallization took place, the overhead stirring speed was maintained at 120 rpm. During the subsequent cooling and crystallization phase, the stirring speed was dynamically adjusted between 100 rpm and 155 rpm to provide continuous mechanical shear. Simultaneously, an external temperature-controlled circulating water bath was activated with the set temperature decreased to 10 °C. Through this efficient thermal exchange, the formulation was cooled from approximately 71.5 °C to 25.7 °C over a period of 72 minutes. This targeted temperature drop actively drove the lipid molecules to overcome the nucleation energy barrier, inducing crystallization.

- Batch 2(500g scale): In an IKA LR 1000 reactor, a homogeneous primary emulsion was prepared. This process utilized a similar feeding sequence and heating method. Due to less efficient surface mixing in this specific equipment, the heating phase was slightly extended to ensure the complete melting of all lipid components, with the mixture temperature temporarily reaching approximately 78 °C. Unlike Batch 1, high-shear homogenization was not applied. Furthermore, vacuum degassing was not performed due to equipment limitations at that time. During the cooling and crystallization phase, the stirring speed was dynamically adjusted among lower ranges (specifically varying between 50, 60, 80, 90, and briefly 120 rpm) to adapt to the increasing viscosity and surface mixing conditions. The IKA LR 1000 equipment lacked a forced cooling jacket, meaning the formulation

relied entirely on natural passive heat dissipation from the high-heat-capacity metal block. Consequently, the formulation underwent a significantly prolonged cooling process; for instance, it took approximately 3.5 hours for the system to cool from the mixing temperature down to 31.7 °C.

4.3.2 Industrial Scale Batches

The macroscopic manufacturing of the industrial-scale batches (Samples A, B, and C) was entirely completed on the standard production line at Bioglan AB. Within this process, the dynamic history of the formulations, such as the cooling rate profile after passing through the homogenizer and the pumping shear frequency in the intermediate pipelines, was continuously recorded by the industrial online monitoring system.

4.4 Analytical Characterization

4.4.1 Rheological Characterization

All rheological measurements were performed on a Kinexus rotational rheometer at LTH using a stainless-steel cone-and-plate geometry, 40 mm diameter, 2° cone angle (CP 2/40). The initial target gap was 0.0788 mm; the working gap during measurement was 0.0716 mm, corresponding to the truncation height of the cone. Each sample was measured once.

The temperature was held at 25.0 °C by the lower-plate Peltier system throughout all tests. Before each test sequence, samples rested on the plate for 300 s to allow stress from loading to relax. Each sample was measured once; the Kinexus rheometer at LTH was used for all rheological measurements reported in this study.

Sample Loading and Shear History

Given the high sensitivity of the lamellar gel network to external mechanical forces, transferring the sample from the packaging container to the lower plate of the rheometer inevitably causes varying degrees of mechanical damage to the matrix. In this study, three distinct loading modes were authentically recorded based on different sampling formats. These specific modes were carefully considered in the subsequent analysis:

- Tube-packaged samples: For Sample B, Sample C, and manually filled tube samples, the formulation was directly extruded from the tube onto the center of the test plate by applying a steady and slow external force. This process primarily introduced extrusion and extensional stress.

- Jar-packaged samples: For the industrial batches with a moderate texture, a sampling spatula was used to scoop the sample. The convex back of the spatula was then utilized to gently rub and attach the formulation to the lower plate. This specific process introduced localized shear and yielding.

- Extremely hard samples: For the cooling-failed industrial batch (Sample A), which possessed an extremely hard texture similar to solid butter, standard spatula loading would prevent the geometry from lowering smoothly to the target gap. Therefore, after being scooped onto the plate, this sample had to be manually and forcefully smeared and thinned using a tool. This operation introduced severe and directional shear damage. Consequently, it could potentially lead to localized heterogeneity.

Each sample was characterised through the following four tests:

- Amplitude Sweep with LVR plus Strain Frequency Sweep: This is an automated continuous testing sequence. Initially, an amplitude sweep was conducted at a constant frequency of 1 Hz over a predefined shear stress range. The system was programmed to automatically terminate this sweep once the linear viscoelastic region was identified. Subsequently, the software autonomously selected a safe strain value within the determined LVR. Using this dynamically assigned strain, a frequency sweep was immediately executed, which decreases logarithmically from 100 Hz to 0.1 Hz to evaluate the frequency-dependent behavior of the moduli and identify any potential crossover points.

- Yield Stress Test: steady continuous flow mode. A shear stress ramp was applied from 0.1 Pa upward at a logarithmic rate. The static yield stress was identified from the peak in the apparent viscosity–stress curve (peak viscosity method). The upper stress limit was set high enough to ensure the sample had passed the yield point and was flowing.

- Flow Curve Test: Utilized a steady-state rotational rheology template. The shear rate was continuously increased from 0.1 s-1 to 100 s-1. The decay trajectory of the system's apparent viscosity was continuously recorded to characterize the pseudoplastic shear-thinning behavior of the formulation after exceeding the yield point.

- Thixotropy Test (3ITT): Employed a three-interval step-shear program based on a continuous rotational mode (R-R-R mode) to quantitatively evaluate the mechanical breakdown and self-healing capacity of the structure:

  First phase: A low shear rate of 0.1 s-1 was applied for 60 seconds to record the baseline apparent viscosity of the sample in a resting state.

  Second phase: The shear rate was instantaneously increased to 100 s-1 and forcibly maintained for 30 seconds. This step simulated the complete structural collapse state during high-pressure pumping or vigorous application.

  Third phase: The shear rate was instantaneously switched back to the low level of 0.1 s-1. The system was continuously monitored for 300 seconds to record the kinetic trajectory of the apparent viscosity climbing over time. This data was used to calculate the recovery ratio of the structure.

4.4.2 Polarized Light Microscopy

The microstructure of the lamellar gel network and the arrangement of the lipid crystals were imaged on an Olympus optical microscope with crossed polarising filters (polariser above the light source, analyser above the objective). This setup visualises the birefringence of the lipid crystals.

Sample Preparation: a small amount of cream was placed on the corner of a clean glass slide and then pushed across the slide with the edge of a coverslip to form a thin, semi-transparent film.

The smearing step introduces a directional shear into the sample, which can locally fracture the lamellar network or reorient it along the smearing direction. This shear history was taken into

account when interpreting the PLM images, especially in relation to crystal orientation and skeleton continuity. Imaging was carried out at room temperature with a 20× objective.

4.5 Ageing and Storage Conditions

To evaluate the impact of process history on the long-term mechanical stability of the network, this study conducted time-dependent rheological tracking for each batch.

All samples, upon preparation or receipt, were uniformly sealed and stored in a controlled room-temperature environment (approximately 20–25 °C) under standard relative humidity. The rheological testing time points were systematically defined into two main stages:

- Initial state (tinitial): The first rheological characterization was completed within 72 hours after the sample was delivered to the laboratory. This test aimed to capture the baseline kinetic characteristics of the crystalline network during its initial formation stage.

- Aged state (taged): All samples underwent a unified rheological re-testing on May 15. Due to the differences in the actual production dates of each batch, the samples experienced varying absolute ageing days upon re-testing. Specifically, this resulted in approximately two months, one and a half months, and two weeks of ageing, respectively.

5 Results

5.1 Rheological Baseline: A Cross-Formulation Comparison

To establish a comprehensive rheological baseline for topical semi-solid formulations, this study selected three classic reference products. These include a gel (ACO Acnegel), a cream (Helosan), and an ointment (Vaselina Pura Reig). A multi-dimensional evaluation was then conducted to compare these references with the commercial target product, Zalve®, which relies on a lamellar gel network (LGN). The key rheological parameters are summarized in Table 5.1.

Table 5.1 Comparative rheological parameters of reference formulations and Zalve®

Formulation type	Reference product	G' LVR (Pa)	tan δ	τy static (Pa)	η3 (Pa·s)[1]	Recovery%[1]
Gel	**ACO Acnegel**	12.2	2.303	N/A	8.1	99.6%
Cream	**Helosan**	2766	0.444	14.3	25.1	66.7%
Ointment	**Vaselina Pura Reig**	11154	0.536	33.4	135.9[2]	100%[2]
LGN cream	**Zalve®**	8940	0.534	2.74	31.1	50.5%

1.Thixotropy protocol: $\dot{\gamma}_1$ = 0.1 s^{-1} (60 s) → 100 s^{-1} (30 s) → 0.1 s^{-1} (300–600 s). η_3 = mean viscosity over the last 30 s of Phase 3.

2. Ointment thixotropy was measured at $\dot{\gamma}$ = 0.5 s^{-1} (non-standard); η_3 and Recovery% are therefore not directly comparable to other formulations and are provided for reference only.

The storage moduli (G') of these reference formulations exhibit a significant stepwise distribution. This precisely illustrates the progression of microstructural network strength from a liquid-dominated to a solid-dominated state. The gel (G' = 12.2 Pa, tanδ = 2.30) behaves as a viscoelastic liquid in the resting state, as evidenced by the loss modulus exceeding the storage modulus (tanδ > 1). In contrast, the cream and the ointment exhibit robust solid-like mechanical characteristics. The ointment (G' = 11154 Pa, tanδ = 0.536) derives its rigidity from a dense network of lipid microcrystals. The cream (G' = 2766 Pa, tanδ = 0.444) occupies an intermediate position.

Interestingly, Zalve® (G' = 8940 Pa, tan δ = 0.534) falls between the cream and the ointment in storage modulus, while tan δ ≈ 0.53 indicates that the elastic response dominates over the viscous one.

Beyond fundamental structural rigidity, this study also evaluated the yield stress and thixotropy recovery capacity of the samples. This evaluation aims to directly correlate microstructural mechanics with the macroscopic clinical application experience. The yield stress determines the critical force required to initiate the flow of a formulation. Test results show that the gel flows even without any stress, which means it is very liquid-like. Conversely, the cream and the ointment require much higher stresses of 14.3 Pa and 33.4 Pa, respectively, to undergo yield

deformation. Zalve® exhibits an optimized yield stress of approximately 2.74 Pa, intermediate between the cream and the gel.

Furthermore, the thixotropy data illustrate how each formulation responds to the destructive high-shear episode of skin application. The gel recovers almost completely ($\eta 3$ = 8.1 Pa·s, Recovery = 99.6%), consistent with its simple, reversible cross-linked network. In comparison, the cream shows partial but incomplete recovery ($\eta 3$ = 25.1 Pa·s, 66.7%), reflecting moderate structural reorganisation after shear. Notably, Zalve® demonstrated a moderate thixotropic recovery ratio of 51.1%, reaching a final recovered viscosity of 30.9 Pas. The specific mechanisms by which Zalve® achieves this unique macroscopic balance through its lamellar gel network, along with its dynamic temporal features during the recovery process, will be detailed in Section 5.2.

Finally, the macroscopic flow curves of all formulations were evaluated. All tested samples, including the reference products and Zalve®, exhibited significant shear-thinning behavior. Shear-thinning ensures that the viscosity drops under the applied shear during spreading, which supports even application across the skin.

5.2 The Baseline: Micro- and Macro Properties of Commercial Zalve®

5.2.1 Microstructure of Zalve®

The field of view was filled with a dense and uniform birefringent texture. This presented the typical morphology of a lamellar gel network. Granular birefringent signals, alternating between golden yellow and purple, were continuously distributed across the entire field. The particle sizes were small and highly consistent. Furthermore, there were no visible large crystalline aggregations, bubble inclusions, or phase separation interfaces.

The birefringent texture exhibited a fine, sandy appearance. The golden and purple-blue regions were tightly interwoven at the micro-scale. This reflects a random, isotropic orientation distribution of numerous small birefringent crystalline domains. Different crystalline domains displayed varied interference colors due to their distinct orientations. Their dense and uniform mixed distribution indicates that the lamellar bilayer assembly within this LGN is highly ordered and spatially homogeneous.

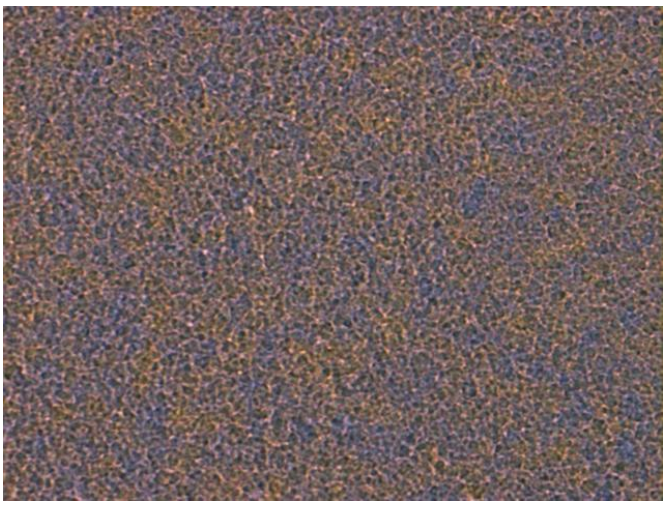

Figure 5.1 Zalve® under PLM

5.2.2 Linear Viscoelasticity and Structural Rigidity

During the dynamic shear-stress-amplitude sweep (controlled shear stress), Zalve® exhibits a broad linear viscoelastic region as shown in Fig 5.2(a). Within the initial plateau region prior to reaching the critical yield point, its storage modulus remains highly stable at approximately 8940 Pa. This value is significantly higher than its corresponding loss modulus. Consequently, this indicates that the system functions as a solid-like elastic network dominated by strong gel rigidity in its resting state.

The subsequent frequency sweep, conducted at a strain amplitude safely within the LVR, reveals that G' increases only weakly with frequency over the range 0.1–100 Hz, following a power-law slope of n = 0.254. This shallow frequency dependence is characteristic of a true, fully developed gel network and demonstrates that the LGN scaffold is mechanically stable across a broad range of deformation timescales. Notably, the G' and G" curves remained highly parallel across the entire investigated frequency spectrum, completely lacking any crossover point.

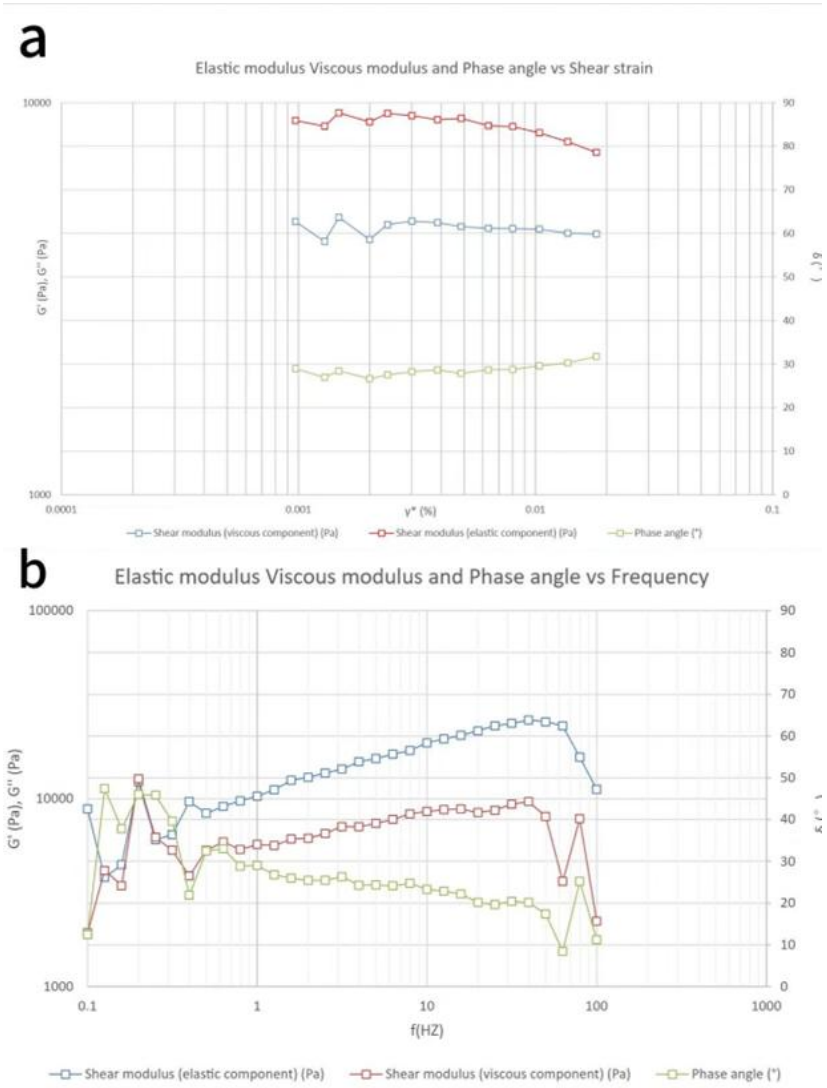

Figure 5.2 Results of oscillation measurement of Zalve® (a) result of amplitude sweep; (b) results of frequency sweep

5.2.3 Yielding Behavior and Thixotropic Kinetics

In the stress ramp test, the apparent viscosity climbed with increasing stress and reached a peak of 6389 Pas at 2.74 Pa, taken as the static yield stress.

Between 7.54 Pa and 7.94 Pa, the apparent viscosity dropped sharply from 3011 Pas to 202 Pas, marking the flow point of the material.

The unique network sensitivity of Zalve® is most convincingly demonstrated in its Three Interval Thixotropy Test (3ITT), as shown in Figure 5.3b. By the second second of Phase 3, the viscosity recovered to 30.9 Pa·s and then stayed nearly constant for the rest of the measurement. The recovery ratio reached 50.5%.

The recovery curve remained essentially flat throughout the rest of the measurement.

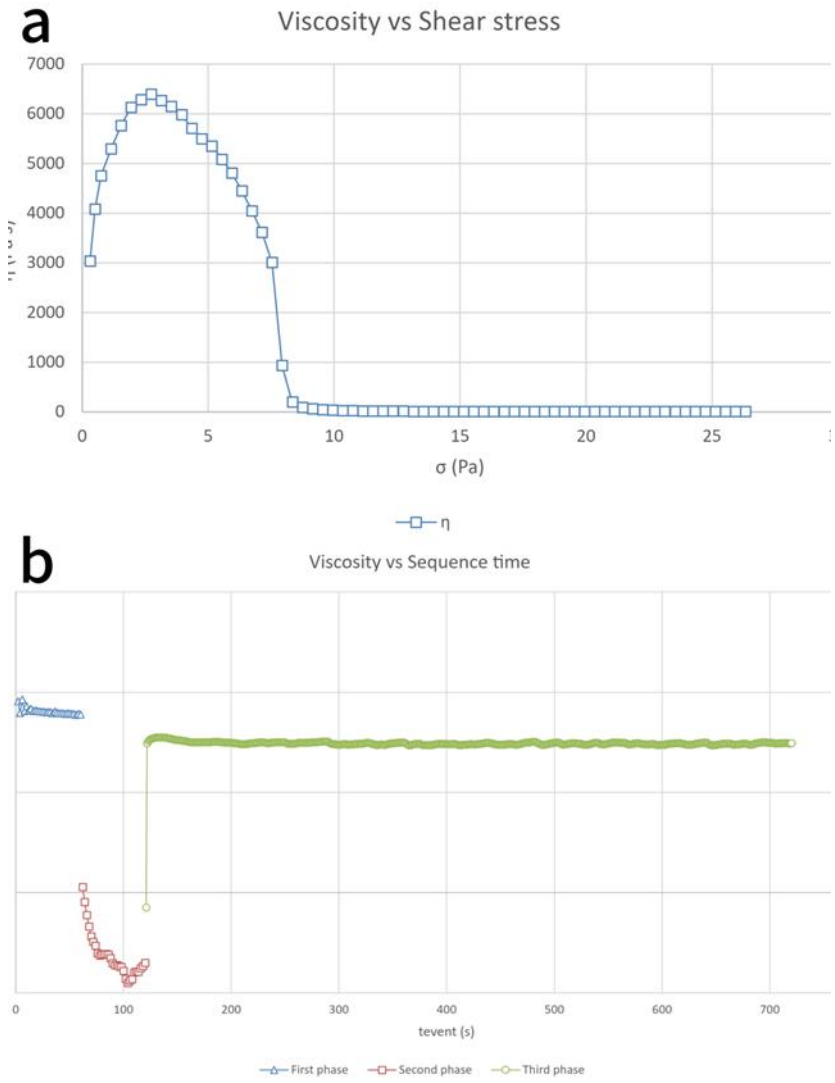

Figure 5.3 (a) result of yield stress test; (b) result of three step thixotropy test

5.2.4 Macroscopic Flow Curve

Finally, the results of the flow curve are presented in Figure 5.4. As the shear rate continuously climbs logarithmically from low to high, the apparent viscosity of Zalve® exhibits a remarkably

smooth and monotonic downward trajectory. This clearly demonstrates highly pronounced pseudoplastic, shear-thinning behavior. The viscosity decreases monotonically with shear rate, confirming shear-thinning behaviour over the full tested range.

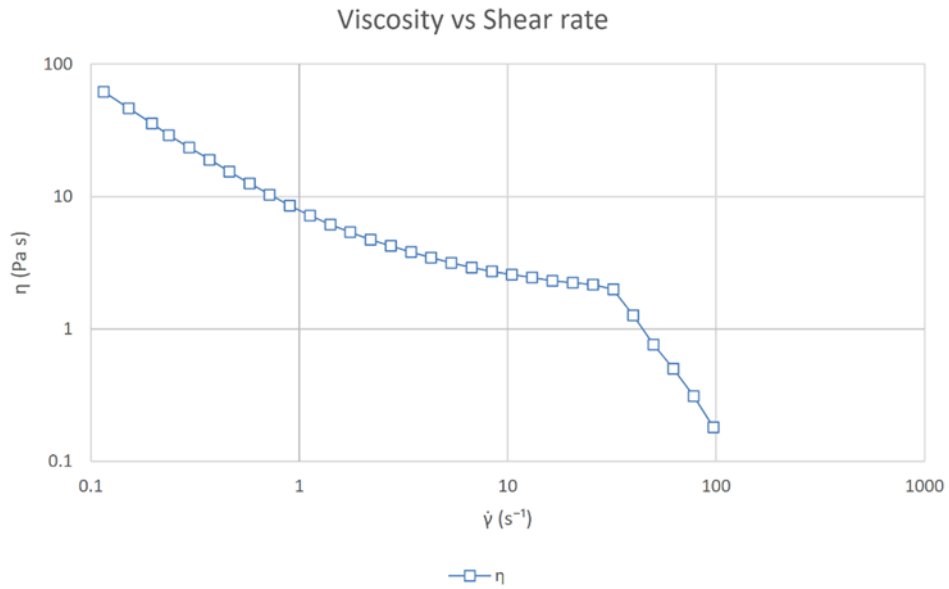

Figure 5.4 Results of alternative flow curve test

5.3 Microscopic and Rheological Behaviour of Two Laboratory-Scale Batches

During the research and development of formulations, the integrity of formulation components and the robustness of the cooling process serve as essential prerequisites for successfully replicating the target microstructure. Before the industrial scale-up, it is important to find the limits of the formulation and process. For laboratory scale Batch 1, a simplified Zalve composition was used with fast cooling process, and for laboratory scale Batch 2, a complete Zalve composition was used with slow cooling process. PLM observations and rheological test results were compared with a commercial sample of Zalve® in Table 5.2.

Table 5.2 Rheological test results comparison among batch1, batch2 and Zalve®

Sample	G' (Pa)	tan δ	τy static (Pa)
Batch 1 (rapid cooling, simplified composition)	13228	0.497	21.0
Zalve® T0 (commercial reference)	8940	0.534	2.74
Batch 2 (slow cooling, complete Zalve® composition)	790	0.913	4.20

5.3.1 Batch 1: Fast Cooling Process

As shown in Fig 5.5a, which is the view of Batch 1 under PLM. The main area of the field of view presented a dense and coarse-grained birefringent texture. Golden-orange and purple-blue colors were distributed alternately across the background. The particle size was significantly larger than that of the commercial Zalve® baseline (Fig 5.1). Additionally, the boundaries between the particles were much more distinct. The overall color saturation and visual contrast were also notably higher. This reflects that the crystalline domains generated during the crystallization process were large and unevenly distributed. Furthermore, an abnormal body was observed in the middle right section of the field. Its interior displayed a mixture of dark green and yellowish-brown colors. This specific texture was clearly different from the surrounding matrix. This structure could be an undispersed lipid crystalline agglomerate.

Rheological tests showed that G' of Batch 1 was high, at 13228 Pa, and the peak yield stress was 21.0 Pa. The apparent viscosity dropped by 95% only when the stress reached about 47.4 Pa, indicating a rigid initial structure with high resistance to spreading. In the 3-ITT, the resting viscosity in Phase 1 was 445 Pa·s. After shear breakdown, the recovered viscosity in Phase 3 was only about approximately 42 Pa·s, resulting in a thixotropic recovery rate of just 9.44%, indicating that the network was unable to recover after shear.

5.3.2 Batch 2: Slow Cooling Process

In contrast to the extreme rigidity exhibited by Batch 1, Batch 2 used slow cooling with a complete formulation. The resulting structure showed weakened mechanical behavior compared to the commercial reference. Fig 5.5b also exhibited a birefringent background. Blue and golden signals covered most of the field of view, indicating the presence of birefringent materials. However, a winding black interface appeared on the right side of the field. To the right of this boundary, a region with significantly weakened birefringent signals emerged. Compared to Batch 1, the granular texture of the birefringence was noticeably coarser. Furthermore, the spatial distribution of the crystalline domains was less uniform. These observations suggest a clear difference in the crystal growth patterns.

The macroscopic data indicated an overall downward shift in the linear viscoelastic modulus of Batch 2. Its storage modulus collapsed to G' = 790 Pa, more than an order of magnitude below Zalve®, and its loss tangent tanδ = 0.913 approached unity, indicating near-liquid viscoelastic character. During the stress sweep, the peak yield stress was merely 4.20 Pa. Furthermore, the flow point stress, defined by a 50% drop in apparent viscosity, was only 8.20 Pa. This indicates that the system is highly susceptible to flow. Due to its overall thin and soft texture, the system recorded a thixotropic recovery rate of 53.90% after undergoing strong shear breakdown. The static viscosity recovered from 69.02 Pa·s in Phase 1 to 37.19 Pa·s in Phase 3.

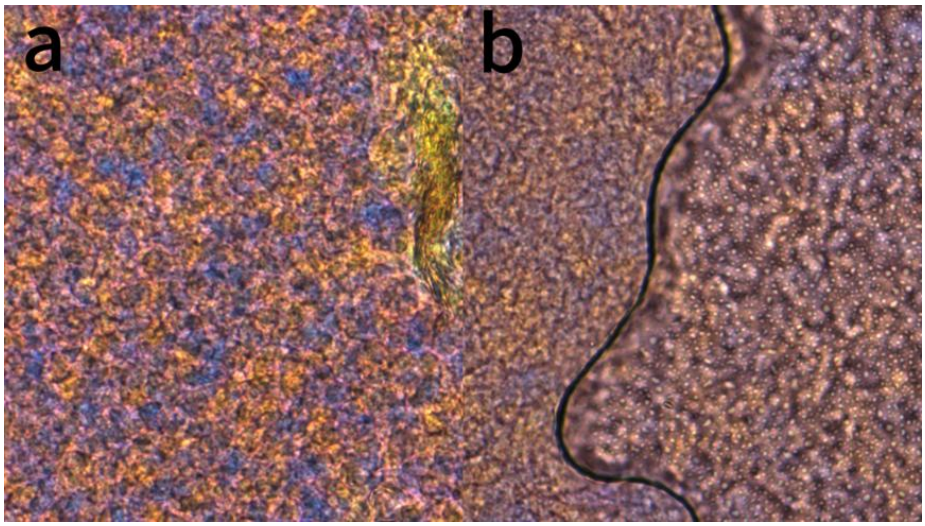

Figure 5.5 (a) batch 1 under PLM; (b) batch 2 under PLM

5.4 Microstructural and Rheological Evolution during Industrial Scale-Up

After the laboratory batches, this section evaluates three industrial samples that represent three distinct process states rather than a sequential time series along the production line: Sample A (incomplete cooling), Sample B (complete cooling but transient discharge with high pump speed), and Sample C (steady-state production).

5.4.1 Inter-Batch Reproducibility

Tables 5.3a–c present the relative percentage differences (RPD) between Batch 02 and Batch 03 for Samples A, B, and C, respectively. RPD thresholds follow the established convention: < 10% equivalent, 10–20% acceptable, 20–30% borderline, > 30% non-equivalent.

The small deformation parameters (G', G", tan δ, and n) consistently fell within the equivalent or acceptable range (RPD < 15%) across all three sampling positions. This indicates a high degree of reproducibility in the steady-state network architecture among the batches. In contrast, the large deformation parameters (τy, η1, and η3) exhibited greater variability. They occasionally crossed into the critical or non-equivalent ranges. This phenomenon was particularly evident in Sample A and Sample C. This dispersion aligns with the fact that large deformation measurements are highly sensitive to the shear history generated during sample loading onto the measurement plate. This manual loading procedure causes minor variations in the localized shear state of the material immediately prior to testing. These variations do not affect the underlying network structure. However, they lead to noticeable deviations in the yield stress and flow viscosity. Although the recovery parameter relies on structural breakdown under large deformation, it remained within the acceptable range (RPD < 20.6%) across all three sampling locations.

Overall, for the purposes of this study, the inter-batch equivalence is considered satisfactory. Therefore, the remainder of this chapter will focus specifically on the data from Batch 02. This specific batch will serve as the representative dataset for the industrial-scale rheological characterization.

Table 5.3a Inter-batch reproducibility of sample A

Sample A — Parameter	Batch 02	Batch 03	RPD (%)
G' LVR (Pa)	44,092	47,169	6.7
G" LVR (Pa)	19,069	20,010	4.8
tan δ	0.432	0.424	1.9
G' slope n	0.203	0.201	1.0
τy static (Pa)	16.6	23.8	35.7
η_1 (Pa·s)	496.7	418.4	17.1
η_3 (Pa·s)	253.7	205.2	21.1
Recovery (%)	51.1	49.1	4.0

Table 5.3b Inter-batch reproducibility of sample B

Sample B — Parameter	Batch 02	Batch 03	RPD (%)
G' LVR (Pa)	30,185	28,622	5.3
G" LVR (Pa)	9,513	9,982	4.8
tan δ	0.315	0.349	10.2
G' slope n	0.181	0.207	13.4
τy static (Pa)	13.4	10.6	23.4
η_1 (Pa·s)	248.6	264.2	6.1
η_3 (Pa·s)	179.4	221.1	20.8
Recovery (%)	72.2	83.7	14.8

Table 5.3c Inter-batch reproducibility of sample C

Sample C — Parameter	Batch 02	Batch 03	RPD (%)
G' LVR (Pa)	13,136	12,211	7.3
G" LVR (Pa)	5,367	4,711	13.0
tan δ	0.409	0.386	5.8
G' slope n	0.245	0.254	3.6
τy static (Pa)	10.6	7.38	35.5
η_1 (Pa·s)	165.8	130.1	24.1
η_3 (Pa·s)	134.8	86.0	44.2
Recovery (%)	81.3	66.1	20.6

5.4.2 Microstructural Evolution during Cooling and Pumping

Polarized light microscopy clearly captured the microstructural evolution of the formulation across different process nodes (Figure 5.7).

The PLM image of Sample A was significantly different from the other samples. Multiple large, coarse birefringent crystalline domains were visible within the field of view. These domains exhibited strong blue and golden-yellow birefringent signals. Furthermore, the boundaries between them were highly distinct. The crystalline domains possessed irregular shapes. Obvious aggregates and block-like structures were present. The color saturation in localized areas was extremely high. This indicates significant differences in crystal orientation. The overall structural heterogeneity was remarkable. This formed a sharp contrast with the fine and uniform crystalline textures of the other samples.

The birefringent texture of Sample B was the most similar to the ordered region of Batch 1. It presented a uniform and fine blue-golden mosaic texture. The crystalline domains were small and evenly distributed. Almost no coarse crystalline aggregates were visible in the field of view.

As shown in Fig 5.7c, the birefringent texture of Sample C was equally uniform and fine. The blue-golden mosaic was widely distributed across the area. The size of the crystalline domains was the smallest among all the samples. The birefringence distribution in the main area was highly uniform. This suggests that Sample C possesses a relatively regular lamellar crystalline network.

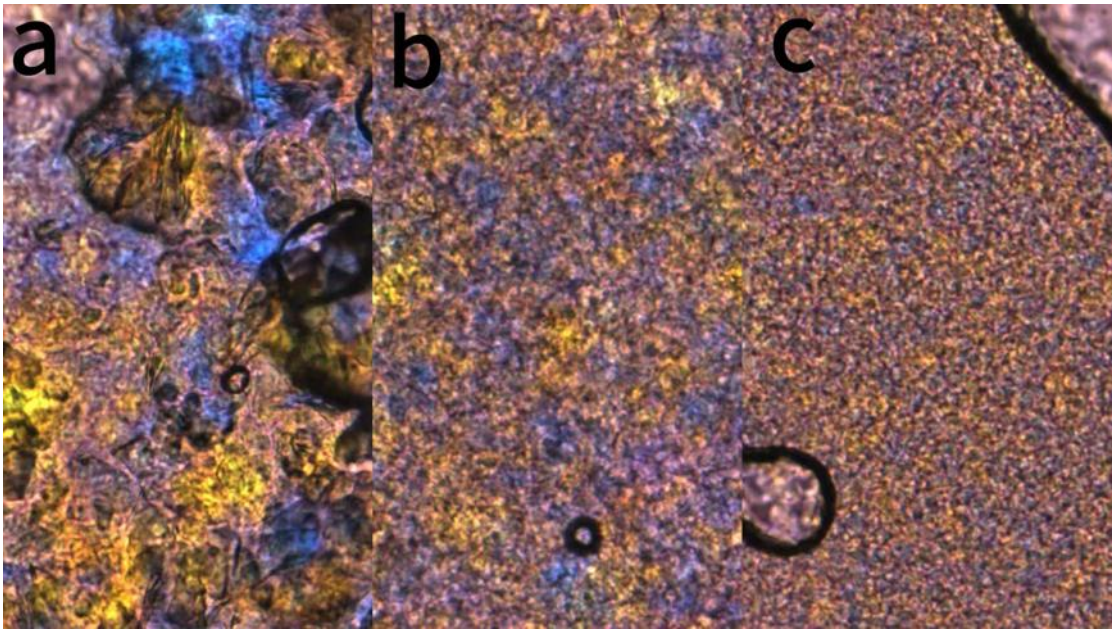

Figure 5.7 Results of microstructure (a) Sample A under PLM; (b) Sample B under PLM; (c) Sample C under PLM

5.4.3 Rheological Characterization

The five rheological tests gave results consistent with the PLM observations. All three samples behaved as solid-like gels (G' > G") across the tested frequency range. The G' values, however, differed widely between the three process states. Sample A, taken at incomplete cooling, contains large crystalline patches and shows the highest G', at approximately 44092 Pa. Sample B,

taken during the transient discharge phase, has G' ≈ 30185 Pa. Sample C, taken during steady-state production, reaches the lowest value, at 13136 Pa.

In the 3-ITT, Sample A shows a recovery rate of 51.5% after high-shear breakdown. Combined with its high initial yield stress (16.58 Pa), this indicates a material with high application resistance. Sample B and Sample C both show lower recovered viscosity and lower yield stress than Sample A, consistent with the lower G' values described above.

To evaluate the state of the finished product as the patient first encounters it, an in-tube sample rested for 48 hours was tested. Extruding the sample from the tube onto the test plate reproduces the extrusion shear experienced during clinical application. The comparison is shown in Table 5.4. After this extrusion step, G' of the in-tube sample reaches 8056 Pa, close to the commercial Zalve® baseline (8940 Pa).

However, its terminal thixotropic recovered viscosity (106.61 Pa·s) and macroscopic yield stress remain significantly higher than those of the commercial benchmark (31.14 Pa·s and 2.74 Pa, respectively). The in-tube sample therefore matches the commercial Zalve® in G' but still differs in the large-deformation parameters at this stage. The implications of this offset are discussed in Section 6.

5.5 Time Evolution Rheological Properties

To evaluate the physical stability of the products from various stages of the production chain, all samples were retested after being stored at laboratory room temperature for a certain period. This section only discusses the key sample data. The polarized light microscopy images of the aged samples are shown in Figure 5.8.

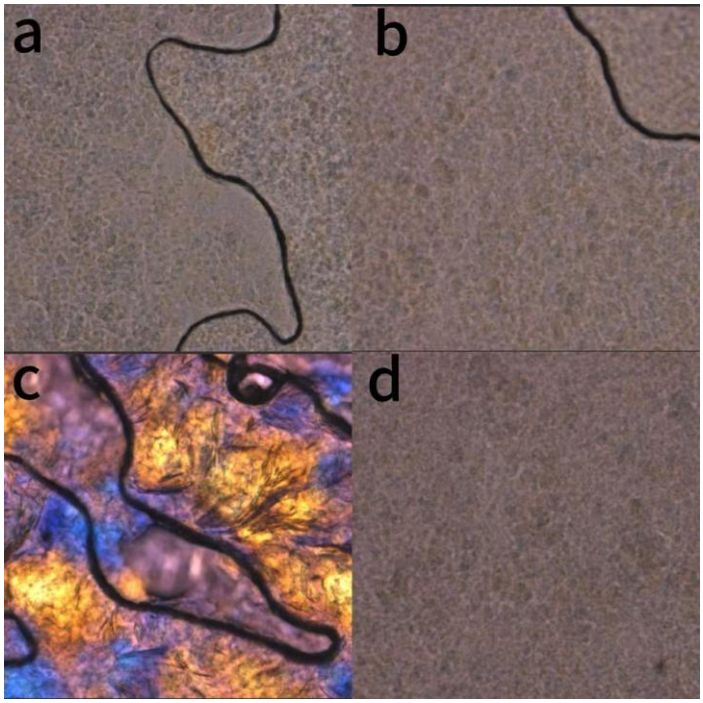

Figure 5.8 Microstructure of aged samples. (a) aged Zalve® under PLM; (b) aged sample C in tube under PLM; (c) aged sample A under PLM; (d) aged sample C under PLM

The commercial Zalve® baseline exhibited significant rheological changes after approximately 70 days of storage. Its storage modulus G' increased from 8940 Pa to 22365 Pa. Tan δ decreased from 0.534 to 0.407. The static yield stress remained basically unchanged, shifting slightly from 2.74 Pa to 2.17 Pa. The thixotropic recovery rate dropped from 50.5% to 21.8%. The recovered viscosity η3 decreased from 31.1 Pa·s to 10.45 Pa·s. PLM images showed that the birefringent colors of the aged Zalve® became paler and less vivid compared to its initial T0 state. The characteristic size of the patches increased slightly. However, the system overall still maintained a uniform birefringent mosaic structure. No phase separation or visible defects appeared.

Sample A was tested after 19 days of storage. Its storage modulus G' increased from 44092 Pa to 47567 Pa. The static yield stress decreased slightly from 16.6 Pa to 14.6 Pa. The thixotropic recovery rate increased from 51.1% to 59.9%. PLM images revealed that the coarse birefringent crystalline aggregates in the aged Sample A were still present. The strong blue and orange-yellow birefringence remained clear. The fibrous internal details were still significant. Nevertheless, the edges of some crystals became smoother compared to their initial state.

Sample C was also tested after 19 days of storage. Its storage modulus G' decreased from 13136 Pa to 9735 Pa. Tan δ increased from 0.409 to 0.471. The static yield stress dropped from 10.57 Pa to 5.78 Pa. The thixotropic recovery rate decreased from 81.3% to 63.4%. PLM images showed that the birefringent colors of the aged Sample C became noticeably paler. The characteristic size of the patches also increased. Despite these changes, the overall field of view remained uniform. No new defects or abnormal structures appeared.

Sample C in tube was tested after 16 days of storage. Its storage modulus G' decreased from 8056 Pa to 6197 Pa. Tan δ increased from 0.426 to 0.461. The static yield stress dropped from 7.78 Pa to 5.38 Pa. The thixotropic recovery rate decreased from 77.5% to 48.3%. PLM images showed that the aged Sample C in tube also exhibited paler birefringent colors and enlarged patches. The overall field of view remained uniform. Visually, the PLM morphology of the aged Sample C in tube was highly similar to the initial T0 morphology of the commercial Zalve®.

Table 5.4 Rheological parameters before and after storage for all characterised samples.

Sample	Storage(days)	G' initial(Pa)	G' aged(Pa)	tanδ initial	tan δ aged	τy static initial	τy static aged	Recovery% initial	Recovery% aged
Zalve®	~70	8940	22365	0.534	0.407	2.74	2.17	50.5%	21.8%
Sample A	20	44092	51162	0.432	0.396	16.6	14.6	51.1%	59.9%
Sample C	20	13136	9735	0.409	0.471	10.6	5.78	81.3%	63.4%

Sample C in tube	18	8056	6197	0.426	0.461	7.78	5.38	77.5%	48.3%

6 Discussion

6.1 Defining Key Parameters at the Laboratory Scale: Formulation Integrity and Crystallization Thermodynamics

Batch 1 lacked key electrolytes such as tetrasodium pyrophosphate. Such electrolytes are known to interact with non-ionic surfactants like PEG-100 stearate through a salting-out mechanism, in which the electrolyte competes for hydration water and thereby alters the surfactant's solubility and partitioning behaviour (Schott & Royce, 1984). While the primary lamellar scaffold is undoubtedly built by the crystallization of monoglycerides, the absence of these electrolytes might partially disturb the interfacial behavior of the PEG-100 stearate co-surfactant. The ionic environment of the aqueous phase is also known to affect the stability of monoglyceride-based lamellar gel networks through multiple competing mechanisms, including bilayer-surface charge effects from ionizable species and screening of electrostatic repulsion by bulk ionic strength (Van de Walle et al., 2008). The absence of tetrasodium pyrophosphate in Batch 1 could plausibly perturb several of these mechanisms simultaneously, and the rheological data alone cannot distinguish their relative contributions.

Batch 1 also showed a “shaving foam” texture caused by air entrained during high-shear crystallisation. Vacuum was pulled to about 700 mBar during the cooling phase, which was not enough to remove the entrained air once lipid crystallisation made the viscosity climb. The high G’ (13228 Pa) and yield stress (21.0 Pa) of this batch are unlikely to originate from the bubbles themselves: Ducloué et al. (2015) showed that gas inclusions in yield-stress fluids tend to lower the storage modulus and leave the yield stress essentially unchanged, rather than raise them. A tentative hypothesis is that the rapid thermal quenching of the primary monoglycerides, potentially compounded by the altered hydration state of the co-surfactant, produced a rigid but poorly organised crystalline network. The bubbles likely then acted as soft inclusions and stress concentrators within this disturbed network, making it prone to brittle fracture under shear, which is consistent with the very low thixotropic recovery rate of 9.4%.

Batch 2 had a complete formulation but slow cooling and low shearing. This gives the lipid molecules time to deposit into large, isotropic crystals (Sato, 2001; Fukushima et al., 1977), and the low shear was insufficient to refine these aggregates. Batch 2 also showed a “shaving foam” appearance because no vacuum was applied, although the lower stirring speed entrained less air than Batch 1. The combination of a coarse, loose crystalline network and trapped air left the system unable to retain water or support its own weight, giving G’ = 790 Pa, tan δ = 0.913, and a yield stress of only 4.2 Pa.

6.2 Industrial-Scale Production: Structural Evolution Along the Process Sequence

The high G’ (44092 Pa) and yield stress (16.6 Pa) of Sample A reflect an incomplete cooling state. The sample was discharged at 33.6 °C, before the full cooling sequence had been completed. At this temperature, parts of the monoglyceride mixture are likely to still have been in a metastable, partly liquid crystalline state, with chain ordering and α-gel consolidation incomplete (the monoglyceride analogue of the $\alpha \rightarrow \beta$ step described in classical fatty-alcohol LGN models by Fukushima et al., 1977). After leaving the production line, the sample cooled passively without further mixing.

The role of shear during cooling in shaping the final microstructure has been demonstrated by Fameau et al. (2024) using in-situ Rheo-SANS on LGN model systems. Their work showed that cooling rate and applied shear jointly control the final bilayer organisation, although the specific case of discharge with interrupted cooling and no further mixing, as in Sample A was not studied directly. The principle is nevertheless consistent with the PLM image of Sample A, which shows large birefringent domains and strong local colour saturation, in clear contrast with the fine mosaics of Sample B and Sample C.

Sample A is therefore not equivalent to Batch 2. Batch 2 failed because slow cooling and low shear ran throughout the entire process, so the LGN structure never developed properly. Sample A, by contrast, had the correct formulation and had passed through the early cooling steps under industrial mixing before being discharged; only the late crystallisation stage was disrupted. The result is a highly heterogeneous but still continuous network, which is why the modulus is high rather than collapsed.

Sample B and Sample C both passed through the complete four-step cooling sequence. They differ in the sampling time and the pump speed during collection. The G' of Sample B (30185 Pa) is lower than that of Sample A but still higher than that of Sample C (13136 Pa), and the gap appears to reflect the action of shear during the maturing of the network. Cunningham et al. (2021) showed that processing conditions, including applied shear rate, influence the final LGN properties such as yield stress, indicating that shear plays a constructive role in network development rather than only breaking the structure down. Sample B was taken during the initial discharge with a higher pump speed, which would be expected to bring the network closer to that of Sample C while leaving the structure denser than in steady-state material. The PLM image of Sample B shows a fine and uniform birefringent texture similar to Sample C, suggesting that the network architecture itself is normal and only the density is elevated.

6.3 Evolution Under Storage Conditions: Three Distinct Aging Trajectories

The aging data collected for Sample A, Sample C bulk, Sample C in tube, and the commercial Zalve® showed three distinct evolutionary trajectories. These differences are not measurement errors. We discuss each trajectory below as a tentative interpretation rather than a fully verified mechanism.

As described in 4.2, the storage time of these samples are different, this study cannot fully rule out that some of the quantitative differences reflect different absolute aging times rather than intrinsic mechanism differences; confirming the trajectories identified here would require a follow-up study with matched aging time points.

6.3.1 Commercial Zalve®

The commercial Zalve® baseline exhibited a 150% increase in the storage modulus G' over approximately 70 days. Simultaneously, the loss factor tan δ decreased from 0.534 to 0.407, and the recovery rate dropped from 50.5% to 21.8%. The direction of these changes, G' increasing, tan δ decreasing, recovery falling, is qualitatively similar to physical aging behaviour reported in colloidal gels and related soft glassy systems. Cipelletti et al. (2000) and Negi & Osuji (2009) showed that the characteristic dynamics and the elastic modulus of fractal colloidal gels evolve slowly with resting time, with universal aging features that parallel those of disordered glassy systems. In a more chemically related system, Nakarapanich et al. (2001) reported that the zero-shear viscosity of cationic surfactant / fatty-alcohol emulsions increases continuously during storage before reaching equilibrium.

We caution that LGN-based creams like Zalve® differ structurally from these reference systems, most notably in containing crystallisable monoglyceride bilayers that can undergo slow α-gel → coagel polymorphic transitions (Heertje et al., 2005). The direction of the observed aging in Zalve® is qualitatively consistent with the literature, but the detailed microscopic mechanism cannot be inferred from these reference systems alone. Direct verification would require structural techniques such as SAXS or DSC, which were outside the scope of this study.

6.3.2 Sample A

Sample A followed the same direction of G' change as the commercial Zalve® (+6%), but its large-deformation behaviour moved in the opposite direction: the static yield stress decreased slightly from 16.6 Pa to 14.6 Pa and the recovery rate rose from 51.1% to 59.9%. This pattern does not match the standard physical-aging response described above for the commercial product.

One tentative interpretation involves slow, room-temperature rearrangement at crystal domain boundaries. Sample A started with coarse, anisotropic crystalline aggregates from interrupted cooling, which are structurally metastable. Fameau et al. (2024) showed that surfactant and bilayer organisation in LGN systems depends sensitively on cooling history; although they studied the cooling step rather than post-production storage, it is plausible that slow, local rearrangements continue at room temperature in initially heterogeneous samples like Sample A, partially smoothing the network over time. The PLM images of aged Sample A do show somewhat smoother crystal edges relative to the initial state, while the coarse domains themselves remain visible. Direct verification of this mechanism would require structural characterisation of aged Sample A by SAXS or Rheo-SANS.

6.3.3 Sample C

Sample C bulk and Sample C in tube evolved in the opposite direction to commercial Zalve® during storage: G' decreased, tan δ increased, and the recovery rate dropped. The samples softened over time. A possible interpretation is that, immediately after passing through the pipes and homogeniser at industrial pump speeds, the freshly collected material is in a transient, mechanically over-loaded state, and that during room-temperature resting the network slowly relaxes toward a less constrained configuration. This is loosely analogous in spirit to the residual stress relaxation reported in colloidal gels following flow cessation (Negi & Osuji, 2009), although the systems are not directly comparable.

The viscosity decay rate during Phase 3 is similar for Sample C bulk and Sample C in tube, which suggests that the long-term relaxation rate is set by the bulk material and is not strongly affected by the tube-filling step. The commercial product, in contrast, has presumably already passed through this early relaxation period during the months between its manufacture and our receipt of it; its later evolution would then be dominated by the densification mechanism described above. After 16 days, the recovery rate of Sample C in tube (48.3%) is close to the commercial T0 baseline (50.5%), but its G' (6197 Pa) is still well below the commercial value (8940 Pa). This suggests that the large-deformation property converges toward the commercial baseline faster than G' does, and that additional resting time would be needed before an in-tube sample matches the commercial product in the linear regime as well.

7 Conclusion

This study used rheological characterization combined with polarized light microscopy to systematically evaluate the microstructural behaviour of a lipid liquid crystalline system (Zalve®) across the dimensions of manufacturing dynamics, processing pathways, and storage time. The results establish a multi-parameter rheological baseline for this semi-solid formulation and provide a basis for using rheology as a diagnostic tool in its industrial scale-up.

First, this study established the steady-state rheological characteristics of Zalve® during continuous industrial production. The steady-state industrial sample (Sample C) exhibited a uniform and fine birefringent mosaic texture, consistent with a spatially homogeneous LGN. It possessed a moderate solid-like elastic character (G' > G") and a balanced yield stress, properties associated with both network stability and clinical spreadability.

Second, regarding process dynamics and deviation diagnosis, the research showed that the assembly of the LGN is sensitive to formulation completeness, cooling rate, and shear history. The laboratory scale demonstrated that the absence of electrolytes (Batch 1) or slow cooling and shear (Batch 2) leads to severe structural deviations: in both cases, coarse or poorly organised crystalline structures developed, accompanied by either excessive rigidification or near-complete collapse of the rheological response. On the industrial production line, incomplete cooling (Sample A) was associated with a heterogeneous network exhibiting an abnormally high storage modulus and elevated application resistance. Together, these results support the use of rheology as a sensitive multi-parameter fingerprint tool for Q3 equivalence assessment and production troubleshooting.

Finally, regarding storage evolution, the study identified three distinct aging trajectories among the samples examined. The commercial Zalve® baseline showed an increase in storage modulus and a decrease in thixotropic recovery, in a direction qualitatively consistent with physical aging behaviour reported in related soft solid systems. The early-stage production-line batch (Sample A), starting from a heterogeneous network with coarse crystalline aggregates, evolved in a different direction with a marked decrease in yield stress and partial recovery of network flexibility, which possibly reflects slow, room-temperature rearrangement of the initially metastable structure. The freshly collected steady-state product (Sample C) softened over time, possibly reflecting relaxation from a transient, mechanically over-loaded state shortly after production. These observations are based on samples with different absolute storage times due to project-imposed constraints, and the proposed mechanistic interpretations are tentative; confirming them would require further studies with matched aging time points and complementary structural techniques. Nevertheless, the existence of multiple distinct aging directions within the same product family underlines that rheological evaluation of LGN-based semi-solid formulations should be conducted at well-defined maturity time points when assessing long-term shelf-life stability.

8 Future Work

Although this study has examined the relationship between the microstructure and the manufacturing processes of the lamellar gel network in Zalve®, several directions remain worthy of further exploration.

- Long-term stability and polymorphic evolution with matched aging time points: The aging observation in this study used a common end date and therefore involved different absolute storage times for the different samples. Future studies could conduct long-term tracking spanning 6 to 12 months across all sample types with matched aging time points, combined with differential scanning calorimetry (DSC), to establish a more complete picture of LGN maturation and a more robust shelf-life prediction.

- In-situ dynamic microstructural characterization: To overcome the limitations of the two-dimensional field of view of PLM and the directional shear introduced during sample preparation, in-situ Rheo-Small Angle Neutron Scattering (Rheo-SANS) or Small Angle X-ray Scattering (SAXS) techniques could be introduced. These methods can simultaneously apply shear and temperature gradients and monitor the dynamic evolution of the bilayer structure in real time at the nanoscale, which would help directly test the mechanistic interpretations proposed in this study.

- Translation into industrial Process Analytical Technology: This study has shown that specific rheological parameters, including yield stress and thixotropic recovery rate, are sensitive to process fluctuations. Future research efforts could focus on converting these offline “rheological fingerprints” into in-line monitoring indicators on the production line, supporting a smarter Quality by Design (QbD) control system.

- Correlation between physical properties and clinical efficacy: The ultimate goal of topical drug delivery is to achieve effective drug permeation. Future research could integrate the rheological properties characterised in this thesis with in vitro drug release experiments, to evaluate the impact of microscopic network strength on drug release dynamics and patient sensory experience.

9 References

1. Ali, A., Skedung, L., Burleigh, S., Barraud-Krauze, H., Rutland, M. W., & Bhanu, P. (2022). Relationship between sensorial and physical characteristics of topical creams. International Journal of Pharmaceutics, 613, 121370. https://doi.org/10.1016/j.ijpharm.2021.121370

2. Awad, T. S., Johnson, D. W., Bureiko, A., & Olsson, U. (2011). Colloidal Structure and Physical Properties of Gel Networks Containing Anionic Surfactant and Fatty Alcohol Mixture, 32(6), 807–815. https://doi.org/10.1080/01932691003756141

3. Barry, B. W., & Saunders, G. M. (1970). The self-bodying action of the mixed emulsifier cetrimide/cetostearyl alcohol. Journal of Colloid and Interface Science, 34(2), 300-315.

4. Barry, B. W., & Saunders, G. M. (1972). Rheology of systems containing cetomacrogol 1000—cetostearyl alcohol. II. Variation with temperature. Journal of Colloid and Interface Science, 38(3), 626-632.

5. Cipelletti, L., Manley, S., Ball, R. C., & Weitz, D. A. (2000). Universal aging features in the restructuring of fractal colloidal gels. Physical Review Letters, 84(10), 2275–2278. https://doi.org/10.1103/PhysRevLett.84.2275

6. Cunningham, G. E., Alberini, F., Simmons, M. J. H., & O'Sullivan, J. J. (2021). Understanding the effects of processing conditions on the formation of lamellar gel networks using a rheological approach. Chemical Engineering Science, 242, 116752. https://doi.org/10.1016/j.ces.2021.116752

7. Ducloüé, L., Pitois, O., Goyon, J., Chateau, X., & Ovarlez, G. (2015). Rheological behaviour of suspensions of bubbles in yield stress fluids. Journal of Non-Newtonian Fluid Mechanics, 215, 31–39. https://doi.org/10.1016/j.jnnfm.2014.10.003

8. European Medicines Agency. (2018). Guideline on quality and equivalence of locally applied, locally acting cutaneous products (EMA/CHMP/QWP/708282/2018). European Medicines Agency.

9. Fameau, A.-L., Veronico, L., Le Coeur, C., Mahmoudi, N., & Gentile, L. (2024). Shear and cooling effects on lamellar gel network structure: Insights from Rheo-SANS. Journal of Molecular Liquids, 414, 126283. https://doi.org/10.1016/j.molliq.2024.126283

10. Fukushima, S., Yamaguchi, M., & Harusawa, F. (1977). Effect of cetostearyl alcohol on stabilization of oil-in-water emulsion: II. Relation between crystal form of the alcohol and stability of the emulsion. Journal of Colloid and Interface Science, 59, 159-165.

11. Goggin, P. L., He, R., Craig, D. Q., & Gregory, D. P. (1999). An investigation into the supramolecular structure of ternary gel systems using oscillatory rheometry, microscopy, and low frequency dielectric spectroscopy. Journal of pharmaceutical sciences, 88(7), 661-669.

12. Nakarapanich, J., Barameesangpet, T., Suksamranchit, S., Sirivat, A., & Jamieson, A. M. (2001). Rheological properties and structures of cationic surfactants and fatty alcohol

emulsions: Effect of surfactant chain length and concentration. Colloid and Polymer Science, 279, 671–677. https://doi.org/10.1007/s003960000470

13. Negi, A. S., & Osuji, C. O. (2009). Dynamics of internal stresses and scaling of strain recovery in an aging colloidal gel. Physical Review E, 80(1), 010404. https://doi.org/10.1103/PhysRevE.80.010404

14. Ribeiro, H. M., Morais, J. A., & Eccleston, G. M. (2004). Structure and rheology of semi-solid o/w creams containing cetyl alcohol/polysorbate emulsifying wax. International Journal of Cosmetic Science, 26(1), 47–59. https://doi.org/10.1111/j.0412-5463.2004.00195.x

15. Sato, K. (2001). Crystallization behaviour of fats and lipids: A review. Chemical Engineering Science, 56(7), 2255–2265. https://doi.org/10.1016/S0009-2509(00)00458-9

16. Schott, H., & Royce, A. E. (1984). Effect of inorganic additives on solutions of nonionic surfactants VI: Further cloud point relations. Journal of Pharmaceutical Sciences, 73(6), 793–799. https://doi.org/10.1002/jps.2600730622

17. Trommer, H., & Neubert, R. H. H. (2006). Overcoming the stratum corneum: The modulation of skin penetration. Skin Pharmacology and Physiology, 19(2), 106–121. https://doi.org/10.1159/000091978

18. U.S. Food and Drug Administration. (2022). Physicochemical and structural (Q3) characterization of topical drug products submitted in ANDAs: Guidance for industry. U.S. Department of Health and Human Services.

19. Heertje, I., van Duynhoven, J. P. M., Broekmann, I., van Kempen, G. M. P., Goudappel, G.-J. W., Sein, A., & Veeman, W. S. (2005). Microstructural investigation of monoglyceride–water coagel systems by NMR and CryoSEM. Journal of Colloid and Interface Science, 285(2), 703–710.

20. Van de Walle, D., Goossens, P., & Dewettinck, K. (2008). Influence of sodium soap and ionic strength on the mesomorphic behavior and the α-gel stability of a commercial distilled monoglyceride. Food Research International, 41(3), 247–254. https://doi.org/10.1016/j.foodres.2007.12.001

21. Wang, F. C., & Marangoni, A. G. (2015). Effect of intrinsic and extrinsic factors on the stability of the α-gel phase of a glyceryl monostearate–water system. RSC Advances, 5(54), 43121–43129. https://doi.org/10.1039/C5RA05045F

10 Appendix

10.1 Appendix A: Original results of polarized light microscopy

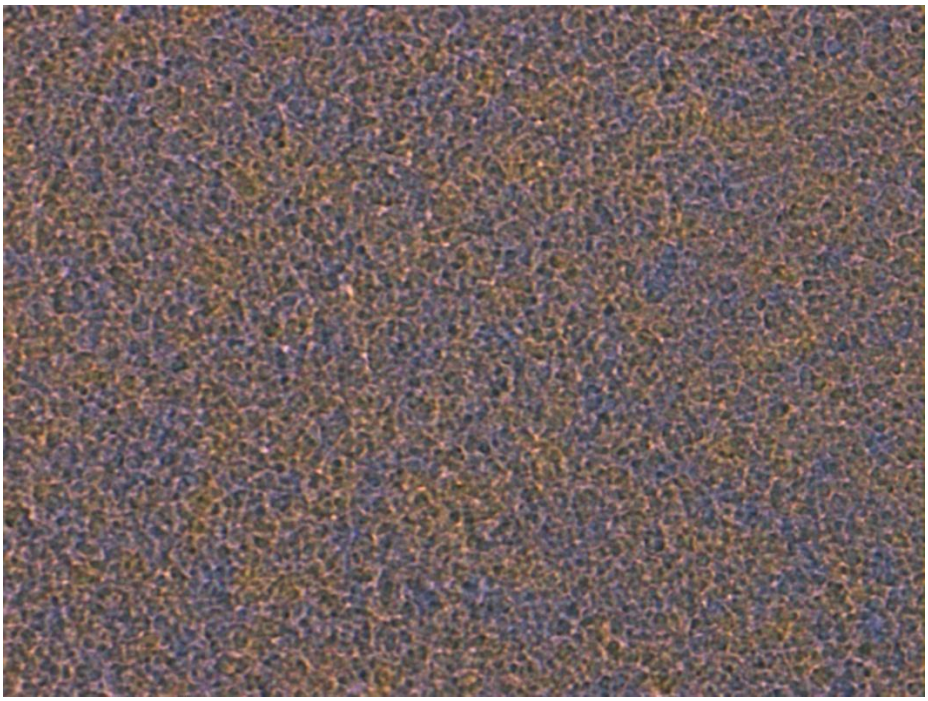

Figure A 10.1 *Zalve® under PLM*

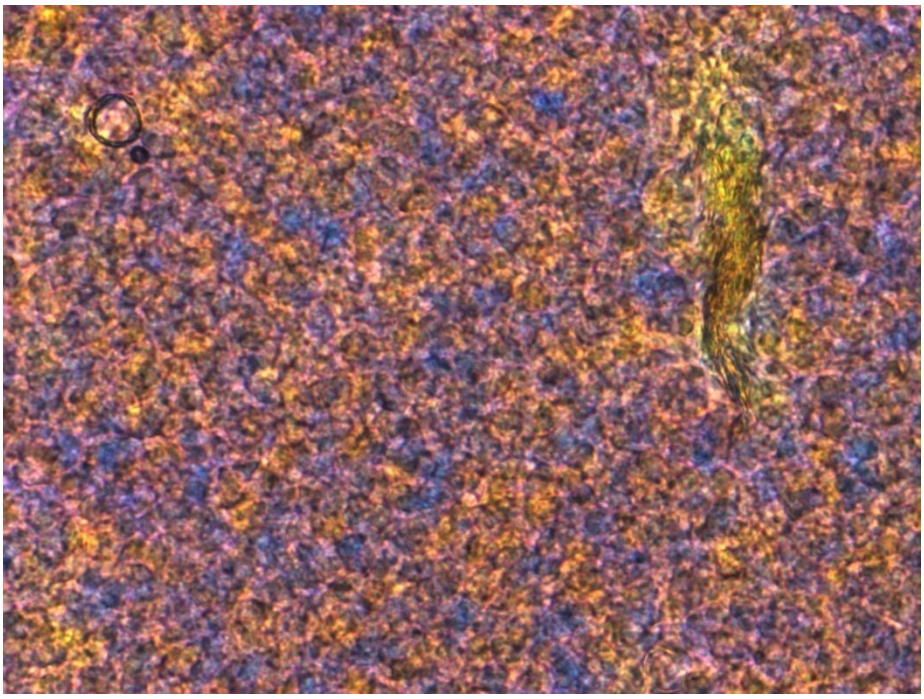

Figure A 10.2 *Batch 1 under PLM*

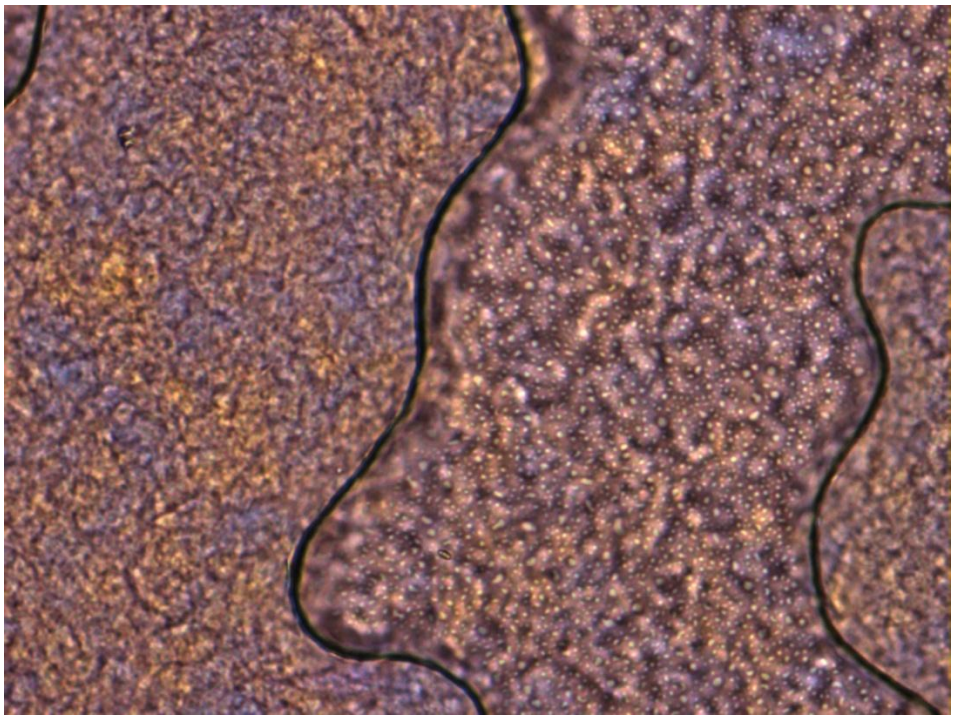

Figure A 10.3 *Batch 2 under PLM*

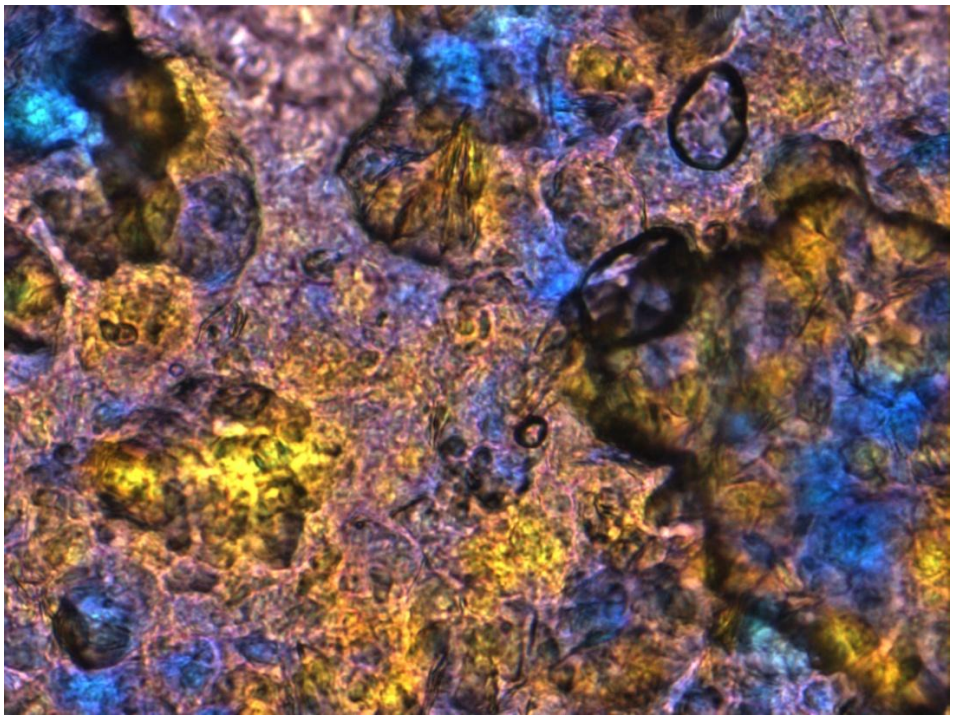

Figure A 10.3 *Sample A under PLM*

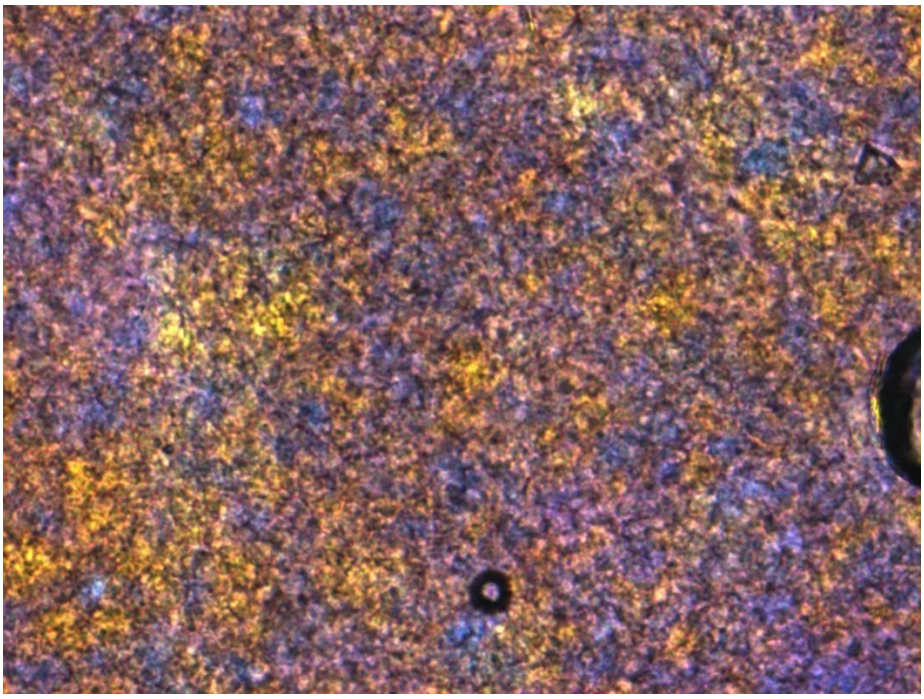

Figure A 10.5 *Sample B under PLM*

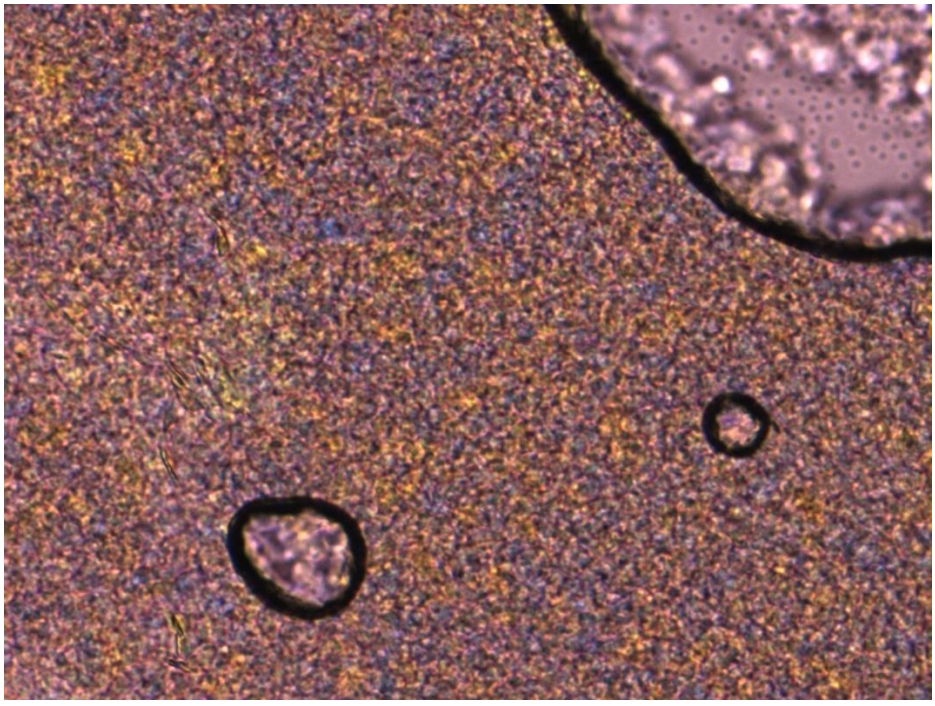

Figure A 10.6 *Sample C under PLM*

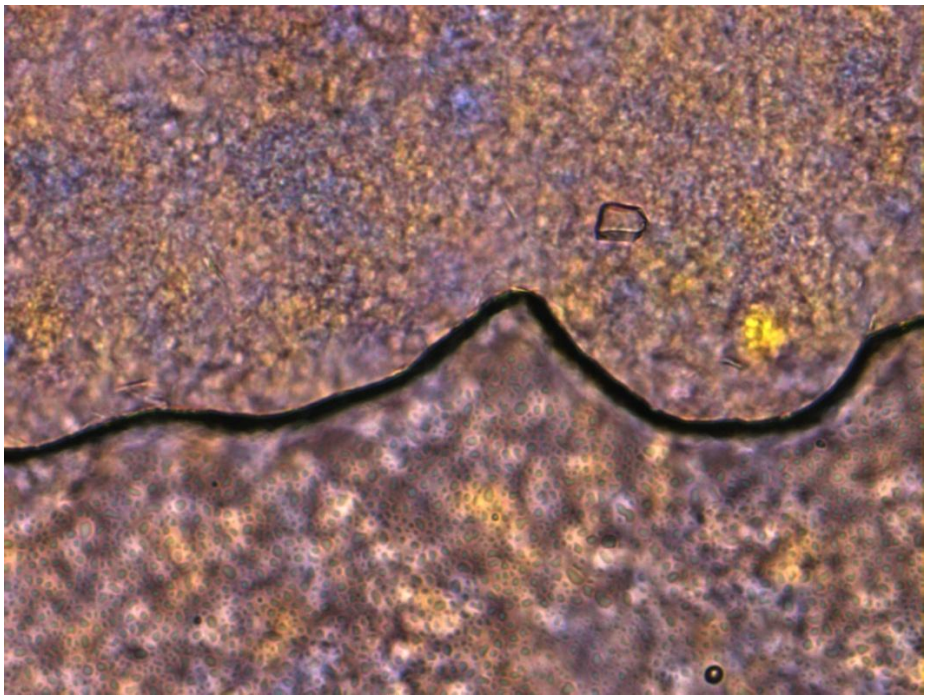

Figure A 10.7 *Sample B in tube under PLM*

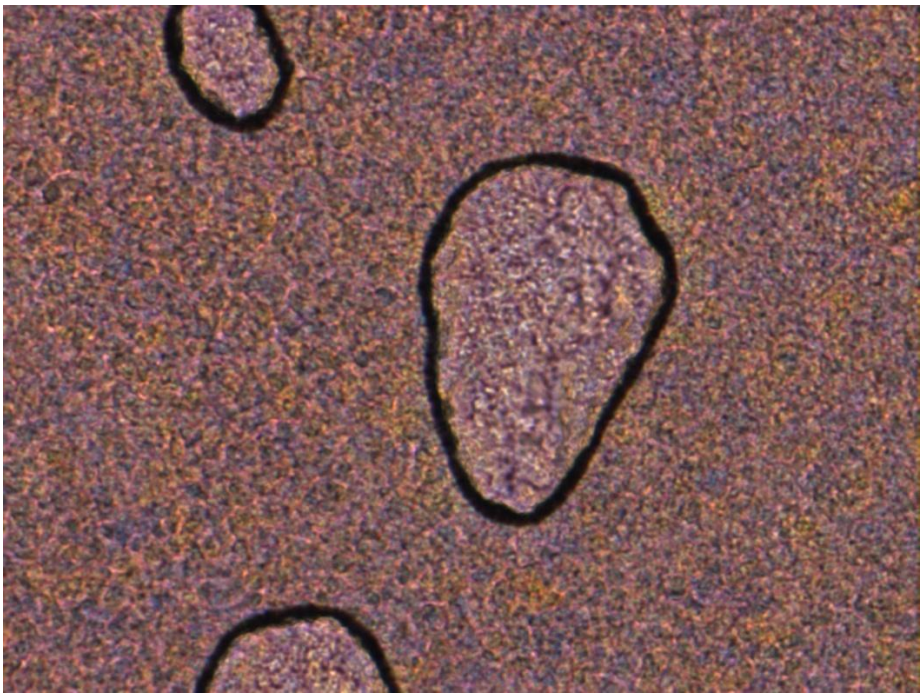

Figure A 10.8 *Sample C in tube under PLM*

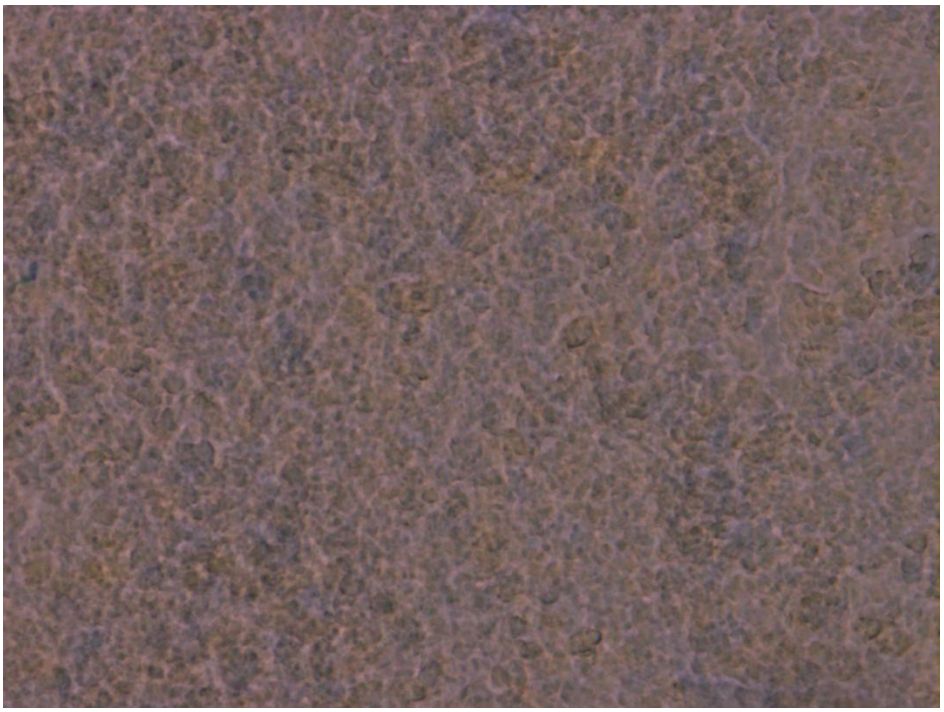

Figure A 10.9 *Aged Zalve® under PLM*

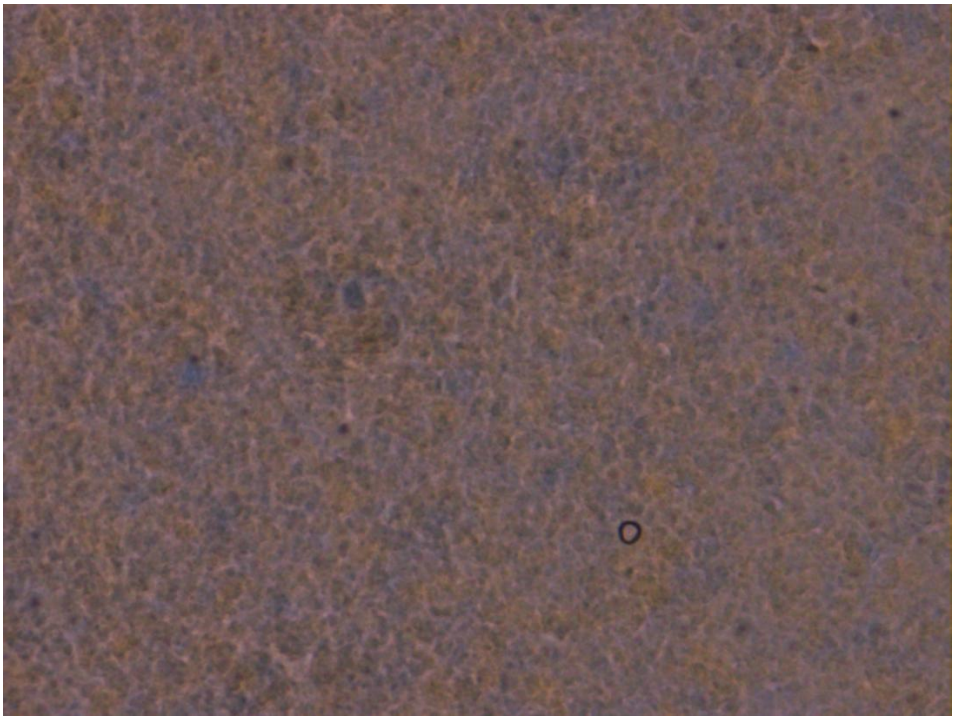

Figure A 10.10 *Aged Batch 1 under PLM*

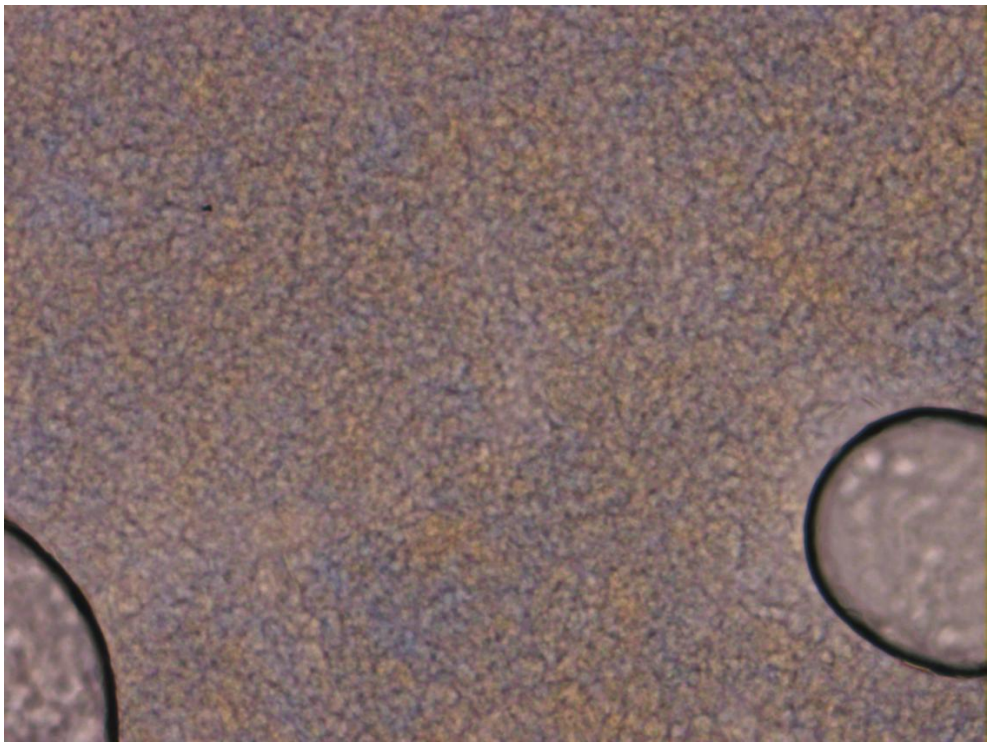

Figure A 10.11 *Aged Batch 2 under PLM*

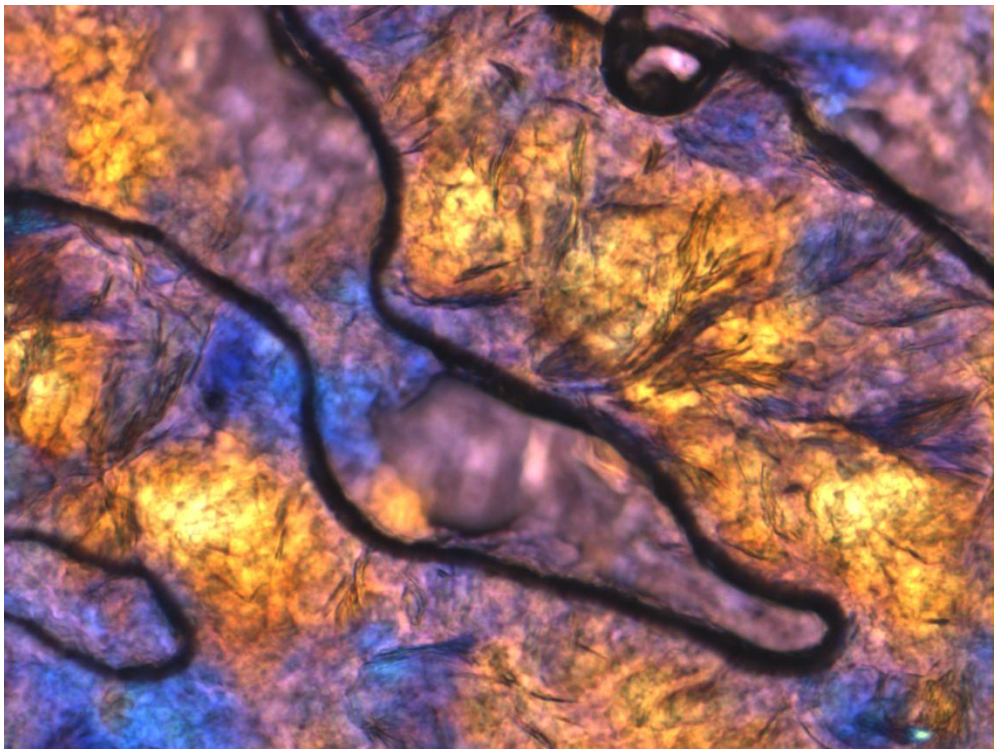

Figure A 10.12 *Aged sample A under PLM*

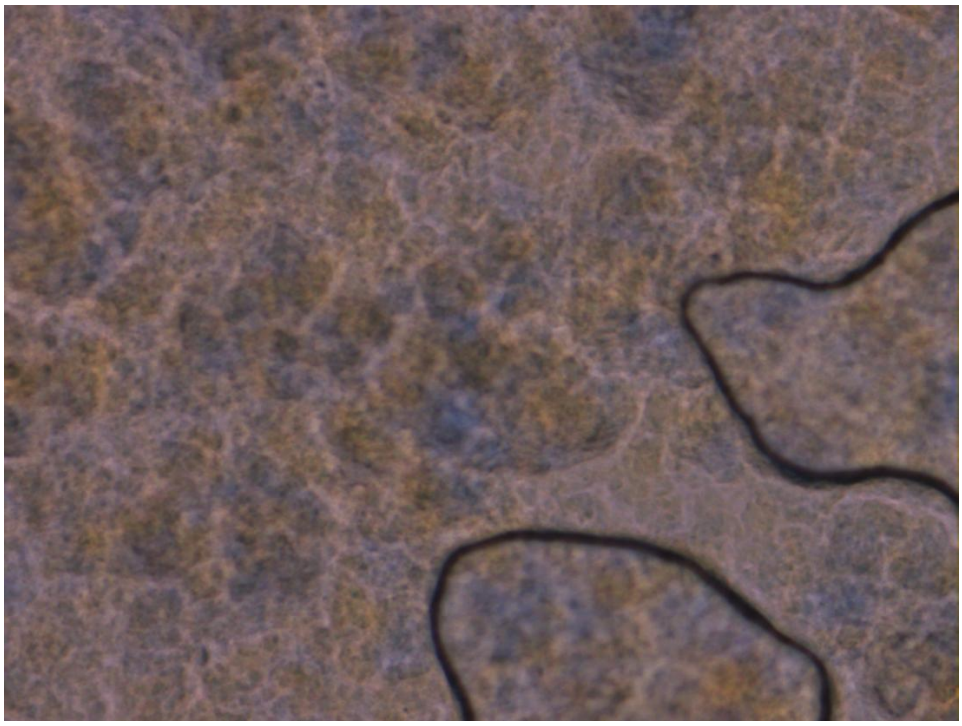

Figure A 10.13 *Aged sample B under PLM*

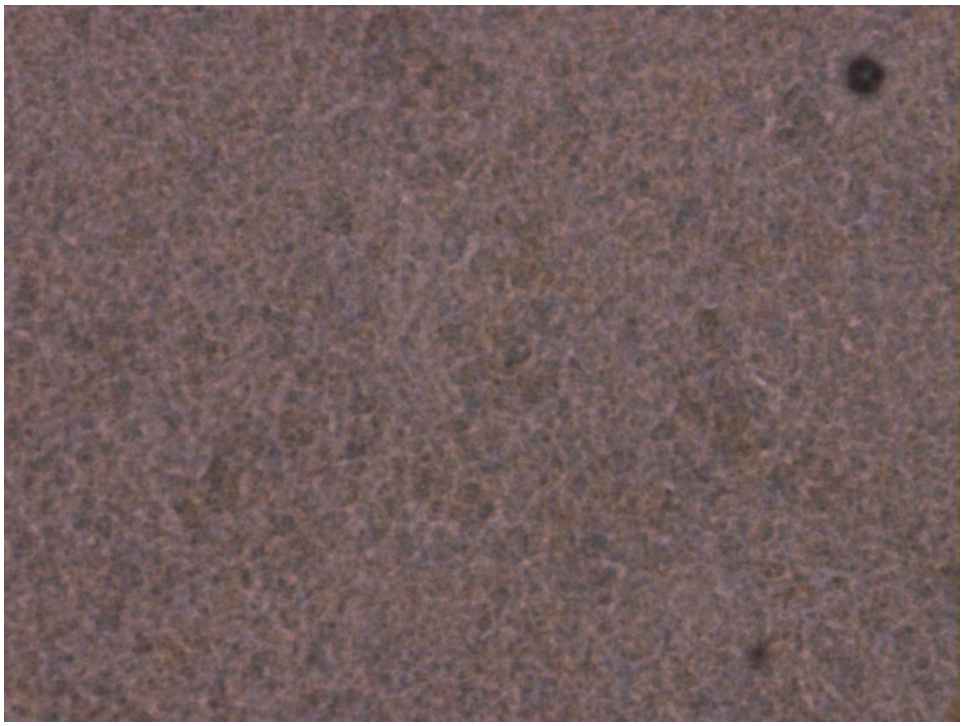

Figure A 10.14 *Aged sample C under PLM*

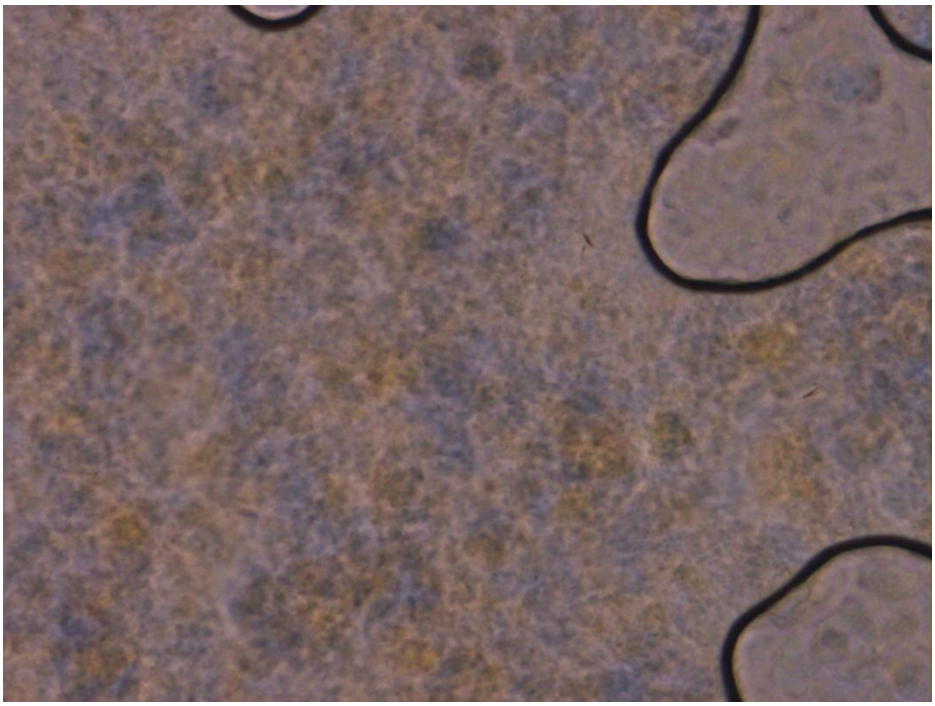

Figure A 10.15 *Aged sample B in tube under PLM*

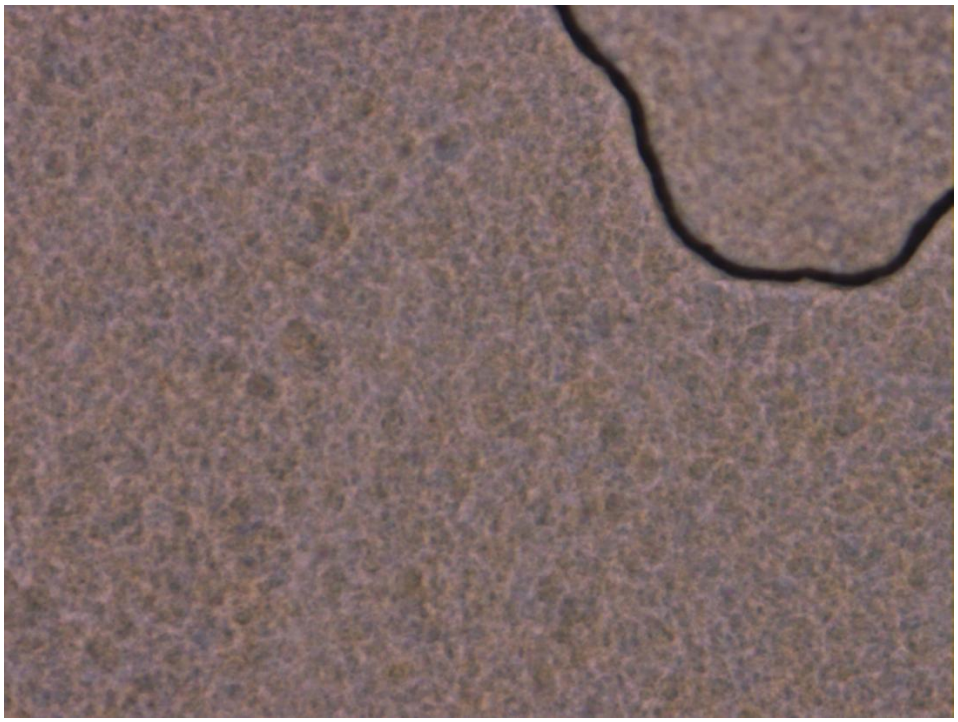

Figure A 10.16 *Aged sample C in tube under PLM*

10.2 Appendix B: Full Rheology data

Table B 10.1 Rheological parameters of all tested samples at the initial state

Sample name	G' /Pa	G" /Pa	tan δ	G' frequency slope n	Yield stress τy/Pa	η_1/Pa·s	η_3/Pa·s	Recovery (η_3/η_1)
Helosan Cream	2766.0	1227.00	0.444	0.208	14.29	37.65	25.13	66.70%
Helosan Gel	12.2	28.13	2.303	0.993	/	8.13	8.1	99.60%
Ointment	11154.0	5974.00	0.536	0.231	33.37	135.1	135.9	100%
Zalve	8938.0	4774.00	0.534	0.254	2.74	61.7	31.14	50.50%
Batch 1	13228.0	6570.00	0.497	0.2428	21	538.24	42.37	9.44%
Batch 2	790.0	721.00	0.913	0.233	4.2	69.02	37.19	53.90%
Sample 02A	44092.0	19069.00	0.432	0.203	16.58	496.66	253.65	51.10%
Sample 03A	47169.0	20010.00	0.424	0.201	23.78	418.4	205.23	49.10%
Sample 02B	30185.0	9513.00	0.315	0.181	13.37	248.64	179.43	72.20%
Sample 03B	28622.0	9982.00	0.349	0.207	10.57	264.18	221.1	83.70%
Sample 02C	13136.0	5367.00	0.409	0.245	10.57	165.79	134.75	81.30%
Sample 03C	12211.0	4711.00	0.386	0.254	7.38	130.11	86.03	66.10%
Sample 02B-tube	22756.0	8262.00	0.363	0.206	11.37	216.5	140.13	64.70%
Sample 02C-tube	8056.0	3428.00	0.426	0.247	7.78	137.58	106.61	77.50%

Notes: All measurements performed at 25 °C using a Kinexus rotational rheometer with a CP 2/40 cone-plate geometry. G', G", and tan δ are mean values over the LVER plateau from amplitude sweep tests. G' frequency slope n is the power-law exponent from log-log fitting of the frequency sweep data. Yield stress τy is determined as the stress at peak viscosity in the stress ramp test. η_1 and η_3 are the average viscosities over the Phases 1 and 3 in the 3-ITT test, respectively. Recovery is calculated as $\eta_3/\eta_1 \times 100\%$.

Table B 10.2 Rheological parameters of all tested samples after storage ageing

Sample name	G’ /Pa	G” /Pa	tan δ	G' frequency slope n	Yield stress τy/Pa	η_1/Pa·s	η_3/Pa·s	Recovery (η_3/η_1)
Zalve	22365.0	9092.00	0.407	0.24	2.17	47.9	10.45	21.80%
Batch1	12910.0	6208.00	0.481	0.275	8.18	287.8	180.4	62.70%
Batch2	2495.0	1698.00	0.681	0.331	3.77	80.56	40	49.70%
SampleA	47221.0	20557.00	0.435	0.203	14.58	321.2	192.4	59.90%
SampleB	39016.0	12250.00	0.314	0.154	6.57	177.6	84.3	47.50%
SampleC	9735.0	4584.00	0.471	0.273	5.78	87	55.2	63.40%
SampleB-tube	23668.0	8669.00	0.366	0.249	4.58	146.33	59.77	40.8%
SampleC-tube	6197.0	2859.00	0.461	0.271	5.38	116.36	56.2	48.30%

Notes: Storage durations between manufacturing and re-testing varied across samples: ~70 days for commercial Zalve®, 56 days for Batch 1, 47 days for Batch 2, 19 days for Samples A/B/C (bulk), 16 days for Sample C-tube and Sample B-tube. All other measurement conditions identical to those described for Table B 10.1.